

DISCLAIMER

This report was prepared as an account of work sponsored by an agency of the United States Government. Neither the United States Government nor any agency thereof, nor any of their employees, makes any warranty, express or implied, or assumes any legal liability or responsibility for the accuracy, completeness, or usefulness of any information, apparatus, product, or process disclosed, or represents that its use would not infringe privately owned rights. Reference herein to any specific commercial product, process, or service by trade name, trademark, manufacturer, or otherwise does not necessarily constitute or imply its endorsement, recommendation, or favoring by the United States Government or any agency thereof. The views and opinions of authors expressed herein do not necessarily state or reflect those of the United States Government or any agency thereof.

Available to DOE and DOE contractors from the Office of Scientific and Technical Information, P.O. Box 62, Oak Ridge, Tennessee 37831; prices available from (615)576-8401, FTS 626-8401.

Available to the public from the National Technical Information Service, U.S. Department of Commerce, 5285 Port Royal Rd., Springfield, Virginia 22161.

Price: Printed Copy A04
Microfiche A01

A STUDY OF SURFACTANT-ASSISTED WATERFLOODING

Final Report

By
John F. Scamehorn
Jeffrey H. Harwell

September 1990

Work Performed Under Contract No. FG22-89BC14449

Prepared for
U.S. Department of Energy
Assistant Secretary for Fossil Energy

Jerry Casteel, Project Manager
Bartlesville Project Office
P.O. Box 1398
Bartlesville, OK 74005

Prepared by
University of Oklahoma
100 E. Boyd, Room F339
Norman, OK 73019

TABLE OF CONTENTS

	Page
LIST OF TABLES.....	iii
LIST OF FIGURES.....	iv
ABSTRACT.....	vi
EXECUTIVE SUMMARY.....	vii
CHAPTER	
I. EXPERIMENTAL VERIFICATION OF SURFACTANT- ASSISTED WATERFLOODING.....	1
1.1 INTRODUCTION AND OBJECTIVES.....	1
1.2 EXPERIMENTAL PROCEDURE.....	1
1.3 RESULTS AND DISCUSSIONS.....	2
II. THEORETICAL MODELING OF SURFACTANT PRECIPITATION IN POROUS MEDIA AND ITS EFFECT ON FORMATION PERMEABILITY.....	3
2.1 INTRODUCTION.....	3
2.2 MATHEMATICAL FORMULATION.....	5
2.2.1 CHROMATOGRAPHIC BEHAVIOR OF SURFACTANT SOLUTIONS.....	5
2.2.2 PHASE CHANGES IN SURFACTANT SOLUTIONS.....	8
2.2.3 VARIATIONS OF PERMEABILITY WITH SURFACTANT PRECIPITATION.....	12
2.3 MODEL VALIDATION BY COMPARISONS BETWEEN THEORETICAL AND EXPERIMENTAL RESULTS....	15
2.4 CONCLUSIONS.....	17
NOMENCLATURE.....	38
REFERENCES.....	41
APPENDIX A : DEVELOPMENT OF AN EMPIRICAL RELATION FOR PERMEABILITY.....	44

LIST OF TABLES

TABLE		Page
1	Composition of synthetic field brine.....	18
2	Characteristics of solid precipitate and SDS/DPC surfactant system.....	19
3	Conditions for the experimental and theoretical work.....	20

LIST OF FIGURES

Figures		Page
1	Effect of dispersion on typical breakthrough curve.....	21
2	Chemical structure of surfactants used in the experimental work.....	22
3	Schematic representation of the equilibrium conditions for an anionic-cationic surfactant system in a porous medium.....	23
4	Theoretical and experimental breakthrough curves for DPC.....	24
5	Theoretical and experimental breakthrough curves for SDS.....	25
6	Phase diagram for the SDS/DPC surfactant system.....	26
7	Lines of r_s superimposed on SDS/DPC phase diagram.....	27
8	Rates of nucleation and growth versus r_s	28
9	Concentration history curves (Run # 1).....	29
10	Concentration history curves (Run # 2).....	30
11	Concentration history curves (Run # 3).....	31
12	Permeability versus pore volumes injected (Run # 1).....	32
13	Permeability versus pore volumes injected (Run # 2).....	33
14	Permeability versus pore volumes injected (Run # 3).....	34
15	Precipitate profiles (Run # 1).....	35
16	Precipitate profiles (Run # 2).....	36

17 Precipitate profiles (Run # 3)..... 37

ABSTRACT

In surfactant-assisted waterflooding, a surfactant slug is injected into a reservoir, followed by a brine spacer, followed by second surfactant slug. The charge on the surfactant in the first slug has opposite sign to that in the second slug. When the two slugs mix in the reservoir, a precipitate or coacervate is formed which plugs the permeable region of the reservoir. Subsequently injected water or brine is forced through the low permeability region of the reservoir, increasing sweep efficiency of the waterflood, compared to a waterflood not using surfactants. Past work has demonstrated the feasibility of this new process for permeability modification in cores and sandpacks without oil present. Background work on surfactant precipitation phase boundaries and adsorption isotherms of surfactants have supported the work. A two-dimensional reservoir simulation model has outlined the promise and limitations of the method.

In this part of the work, two major tasks are performed. First, core floods are performed with oil present to demonstrate the improvement in incremental oil production, as well as permeability modification. Second, a reservoir simulation model will be proposed to further delineate the optimum strategy for implementation of the surfactant-assisted waterflooding, as well as indicate the reservoir types for which it would be most effective.

EXECUTIVE SUMMARY

In surfactant-assisted waterflooding, oil is recovered from the high permeability regions of a heterogeneous reservoir., These regions are then partially or completely plugged by in-situ formation of precipitate. As these plugging zones appear, the injection patterns will change and a larger proportion of the reservoir will then be contacted by the injected fluid, resulting in improved sweep efficiency and ultimately increasing the oil recovery of a secondary or tertiary process.

The work presented here demonstrate oil mobilization and the improvement in incremental oil production, as well as permeability modification when surfactant-assisted waterflooding is used. The selective plug placement of the process is experimentally verified in the high permeability regions of a porous medium which is initially saturated with oil. Moreover, experiments were performed to measure the kinetics of precipitation and precipitate particle sizes as a function of time, since non-equilibrium effects are important in the process. Finally a two-dimensional reservoir simulation model is proposed. The model accounts for precipitation of two oppositely charged surfactants in solution within a porous medium. The novel significance of the proposed mathematical modelling work is that the simulator directly relates the extent of precipitate formation to the permeability reduction due to the plugging of the flow paths by the precipitate particles.

Precipitation processes go through two steps. First, nucleation occurs. The first nuclei which form are relatively small in size so that they are not capable of either blocking the pore throats or reducing the porosity to any extent. Second, growth of the particles occurs due mainly to the supersaturation of the surrounding fluid. When these particles grow large enough, they will either block the pore throats or reduce the local porosity to the extent that significant permeability reductions occur.

To predict the results of laboratory scale experiments, kinetic phenomena and several potential and dominating mechanisms important to the process are examined and incorporated into the model. Factors, such as, rate constants for nucleation and growth are estimated on a per case basis. Equations are defined to account for both mechanisms of precipitation, namely, nucleation and crystal growth. In addition, other mechanisms are considered such as: deposition of precipitate particles on the surface of the media, entrainment of the particles from the surface back into the flowing fluid, movement of the particles in the flowing medium, dissolution of the precipitate particles into the surrounding fluid medium, surfactant adsorption, and chromatographic movement of surfactants are considered. At this

stage, the model is set up for one-directional, two phase flow (water and precipitate) through an initially homogeneous reservoir. The model is able to determine the plug location, size of the plugs, and time to onset of plugging in a reservoir simulation. The results obtained from the kinetic model are compared to core flood data to obtain an empirical relation for the permeability reductions.

CHAPTER 1

EXPERIMENTAL VERIFICATION OF SURFACTANT-ASSISTED WATERFLOODING

1.1 INTRODUCTION AND OBJECTIVES

The objectives of the experiments described in this report are to investigate the permeability reduction in consolidated Berea sandstone cores produced by a selective plugging process and to demonstrate an enhanced oil recovery over normal waterflooding. The process uses phase changes in surfactant solutions and the chromatographic movement of surfactants to improve the volumetric sweep efficiency. High permeability regions are the desired locations for surfactant precipitate formation to occur. The ultimate goal is to plug the high permeability regions and force the fluid flow into the low permeability zones which have a higher oil saturations after waterflooding.

The process begins with injecting a dilute surfactant solution into the core. This surfactant is chosen to have a high electrostatic attraction to the charged surface of the Berea, and, thus, to have a low chromatographic velocity in the porous media. A brine "spacer" is then injected to move the surfactant away from the inlet end of the core and into the water channels between the injection and production wells. A second dilute surfactant solution is then injected. This surfactant has a higher chromatographic velocity in the porous medium due to lower chromatographic attraction to the surface of the medium. When the two surfactant slugs interact in the water channels, they undergo a phase separation. This results in formation of either precipitate or a viscous, gel-like coacervate phase which is capable of blocking partially or completely the high permeability regions in which the wave/wave interference occurs. The subsequently injected fluid will then be forced to pass through the low permeability channels, mobilizing the remaining oil from these regions.

1.2 EXPERIMENTAL PROCEDURE

Berea sandstone cores were stabilized prior to each run. This was required by the presence of considerable amounts of clay minerals, which could migrate or swell to cause plugging. In order to minimize these effects, 100 pore volumes of a 10% synthetic field brine (SFB) solution was injected through each end of the core. The 10% SFB is a dilution of a full strength SFB whose composition is shown on Table 1. Several factors, such as

injectivity rate, salinity, and pH were also monitored and kept constant. Brine solutions were vacuumed filtered and degased in order to prevent fine particles or air bubbles from getting into the system and effecting the apparent permeability. After stabilization, the cores were flooded with an oleic phase. In order to reduce the effect of gravity segregation, the cores were placed in a vertical position and n-heptane was injected into the core downward to displace the water. The injection of the oleic phase continued until an irreducible water saturation was obtained. At this time the cores were returned to the horizontal position and the flow of n-heptane was continued until the pressure drop across the cores reached a steady condition, at which time the effective permeability of the cores to oil was measured. A waterflood was then performed with 10% SFB. The amount of oil recovered at water breakthrough and at the time when the flow of oil stopped was recorded as a fraction of the total oil originally in place. The initial effective permeability of the cores to brine was measured. At this stage surfactant solutions were injected into the core in sequence. Pressure and flow rate were also monitored during the flow experiments.

The precipitation reaction of the anionic surfactant Sodium Dodecyl Sulfate (SDS) and the cationic surfactant Dodecyl Pyridinium Chloride (DPC) was selected as a representative surfactant precipitation reaction.

1.3 RESULTS AND DISCUSSIONS

Several experiments were conducted to show the effect of formation of precipitate on the permeability of the core and to investigate the extent to which the residual oil could be recovered after normal waterflooding.

Even though the starting permeabilities of the sandstone cores in the manifolded system were different by at least an order of magnitude, upon oil saturation and during normal waterflooding, the individual cores exhibited almost similar permeability to water, making the system behave as a homogeneous medium. Therefore no surfactant was injected. The success of surfactant-assisted waterflooding was demonstrated in the first quarterly report on heterogeneous systems. However, when the system is homogeneous, there would be no point of starting the process to change the injection pattern. Any attempt to plug only one core would be unsuccessful as the surfactants invade uniformly throughout the system and phase separation occurs everywhere. Therefore, plugging occurs in both cores with no selectivity for either one.

CHAPTER 2

THEORETICAL MODELING OF SURFACTANT PRECIPITATION IN POROUS MEDIA AND ITS EFFECT ON FORMATION PERMEABILITY

2.1 INTRODUCTION

The precipitation of surfactants has been found to be detrimental in a variety of processes such as pharmaceutical applications of surfactant-dye (1-4), detergency, separation techniques, or even in Enhanced Oil Recovery (EOR) methods (5), where a loss of surfactant from the driving fluid results in inefficiency of the recovery process. In classical surfactant flooding, the injection strategies are designed such that precipitation can be avoided. By so doing, the amount of surfactant available to recover oil is maximized and the interfacial tension is kept low at the oil/water interface. In contrast to the detrimental effects of precipitation in low tension surfactant flooding, there are other surfactant-based recovery techniques in which it is found to be beneficial. One of which is the surfactant-assisted waterflooding method initiated and currently under study in this laboratory (6).

The problem of the natural heterogeneity of reservoir rocks, which results in low volumetric sweep efficiency and leads to the trapping of the oil in the formation, motivated researchers in the area of EOR to investigate selective plugging methods. The idea is to change the injection pattern after a substantial portion of the oil is recovered from these zones and force the subsequently injected fluid to pass through the low permeability regions which have not been previously contacted by injected fluid and which also have a higher oil saturation after normal waterflooding. This is done by blocking the least resistant regions-sometimes referred to as "thief zones". Several potential injection agents such as foams, polymers, microbes, and surfactants are currently in use to correct the preferential invasion of the injected fluid toward the higher permeability regions of a non-homogeneous formation (5-9). But, no matter what agent is used, the plugging of the porous medium is accomplished either by mechanical means, where the flow path is blocked either by coagulated particles or by an assembly of relatively large particles (about 30μ in diameter) at the pore throat (sometimes referred to as "bridging"), or by physicochemical means, where relatively small sized particles (about 1μ in diameter) are deposited to create a coating layer on the surface of the reservoir medium (10).

This chapter presents a mathematical analysis of a novel process that enhances the volumetric sweep efficiency of a reservoir using mixtures of surfactants to plug the high permeability regions. One possible injection strategy consists of sequentially injecting two very dilute surfactant slugs (concentrations on the order of hundredths of a weight percent), with viscosities very little different from brine, into a porous medium with a brine spacer injected between them. The two surfactants and their concentrations are chosen under two conditions: (1) that the first surfactant injected will have a higher electrostatic attraction to the charged surface of the medium and thus will have a lower chromatographic velocity in the reservoir than the second surfactant, and (2) that upon interpenetration of the fast moving front part of the second slug into the slow propagating rear part of the first surfactant slug, a phase separation will occur in the bulk solution or at the admicellar pseudophase. The last condition results in the formation of a solid precipitate, or a viscous, gel-like coacervate phase, resulting in a reduction of the permeability of the region in which the mixing occurs. The experimental evidence for a well defined system and the technical feasibility pertinent to this approach is presented and discussed elsewhere (11).

Much of the work that has been done to establish a model for the process assumed that the phase separation took place instantaneously and that the permeability reductions were arbitrary (12-13); however it has been observed in most cases, including in systems studied by previous investigators, that solutions remain clear for long periods of time before precipitation begins to form. Phase separation in surfactant mixtures, even when the surfactants are dilute and oppositely charged, does not occur instantaneously. It often takes days or even weeks before particles of precipitate appear. There was no previous attempt to quantify the amount of precipitate formed, but rather for any instant of time, the equilibrium state of the mixture was assumed. Another weak point of previous studies was that the solid particles suspended in the flowing fluid were not allowed to move throughout the porous medium. The particles were assumed to be deposited at the sharp interface of the two surfactant slugs where the interpenetration was first started. This resulted in permeability reductions in the same place of fixed magnitude. Dissolution and weakening of plugs were either neglected (13) or considered to occur instantly (12).

The primary goal of this work is to extend the previously established models and to provide a stronger foundation for understanding surfactant precipitation in porous media upon the interaction of pure surfactant solutions. Specifically, the model is set to find out how fast the solid phases are formed, grown, transported, dissolved into the surrounding fluid,

retained to the surface, then entrained back to the flowing fluid inside a porous medium. The success of the model depends on how well the above mechanisms can be predicted and can be related to the variations in local permeability.

2.2 MATHEMATICAL FORMULATION

A macroscopic approach to the process of precipitation of surfactant solutions inside a porous medium was adopted in this study by utilizing mass balance equations and rate equations. The in-situ formation of surfactant precipitate depends on two specific physical phenomena: 1) the chromatographic movement of dilute aqueous surfactant solutions, and 2) the process by which a separate phase emerges from a mixture of two dilute aqueous surfactant solutions. In addition, a third phenomena will be examined which accounts for the observed sharp decline in permeability upon interaction of two surfactant slugs.

2.2.1 Chromatographic Behavior of Surfactant Solutions

When an aqueous surfactant solution is injected into a bed of porous solid, any particular surfactant molecule will move through the medium by spending part of its time adsorbed on the stationary solid surface and part of its time in the mobile aqueous solution. Each molecule of surfactant, and thereby the generated concentration variations (sometimes referred to as "waves") of the adsorbing surfactant component, will propagate through the porous bed at a velocity which is less than the velocity of the carrier fluid. As the equilibrium adsorption of surfactant species increases for a fixed mobile phase concentration, the fraction of total time that each surfactant molecule will spend on the immobile solid surface decreases, thereby, the relative velocity of the propagating surfactant concentration change increases (14,15).

The dominating adsorbate-adsorbent interactions in this study are the electrostatic and hydrophobic driving force which can be modified by changing the structure of surfactant molecules, the surface charge of the substrate, or the electrolyte concentration in the mobile phase.

The surfactant adsorption is approximated here by a simple model proposed by Trogus et al (16). This model suggests that at concentrations below the critical micelle concentration (CMC), the adsorption obeys Henry's law; i.e., the adsorption isotherm has a constant slope below the CMC. At concentrations above the CMC, where according to the phase separation model, any increase in surfactant concentration results in the formation of micellar

aggregates at a constant monomer (unassociated, dispersed molecules) concentration, the total adsorption remains constant. It is further assumed that local equilibrium exists between the mobile aqueous phase and the stationary solid phase. The adsorption of surfactants can be shown as:

$$q = H C_m \quad \text{for } C < \text{CMC} \quad (1)$$

$$q = H (\text{CMC}) \quad \text{for } C \geq \text{CMC} \quad (2)$$

where q is the adsorbed concentration of surfactant, C_m is the monomer concentration, and H is the proportionality or Henry's law constant.

Surfactant adsorption can also be shown in (μM) by the following equation:

$$C_a = H C_m \rho_s (1-\phi)/\phi \quad (3)$$

where ρ_s is the density and ϕ is the porosity of the porous solid.

When brine is injected behind a surfactant slug above its CMC, two new stable concentration variations are produced and begin to propagate from the inlet through the media (14,15). The leading wave is at the injected concentration and the second wave is at the CMC. This behavior is solely dependent on the shape of the adsorption isotherm (16). However, the process of molecular diffusion, dispersion, and or the magnitude of the overall adsorption (small Henry's law constant) have the effect of spreading the waves, especially the wave at the CMC of the surfactant. So, in some cases, it is not possible to distinguish one wave from another (14,17). Figure 1 represents typical breakthrough curves for a particular surfactant at different levels of dispersion. The CMC wave appears only when no dispersion exists. In the case where dispersion does exist ($pe^{-1}=0.2$), the second wave is smeared out.

The surfactants used in this study are the anionic surfactant sodium dodecylsulfate (SDS) and the cationic surfactant dodecylpyridinium chloride (DPC). The chemical structure of these surfactants are shown in figure 2. Figure 3 is a schematic representation of the equilibrium conditions that exists in solutions of cationic/anionic surfactant system in porous media.

The propagation of these surfactants through a porous medium is expressed by a material balance with considerations for the equilibrium conditions between monomer and micelle, adsorbed surfactant, and precipitate. The differential mass balance for the total surfactant is shown by:

$$\frac{dc^T}{dt^+} + \frac{dc}{dx^+} + \frac{dC_{p,b}}{dx^+} + Pe^{-1} \frac{d^2c}{dx^{+2}} = 0 \quad (4)$$

where c^T is the total surfactant concentration and is expressed by the sum of the concentrations of monomer, C_m , micelle, C_M , adsorbed surfactant, C_a , suspended precipitate, $C_{p,b}$, and deposited precipitate, $C_{p,d}$.

$$c^T = C_m + C_M + C_a + C_{p,b} + C_{p,d} \quad (5)$$

C is the solution concentration ($C = C_m + C_M$), while t^+ and x^+ represent the dimensionless time and distance respectively and are defined by:

$$t^+ = \frac{u t}{L} \quad (6)$$

$$x^+ = \frac{x}{L} \quad (7)$$

where u is the velocity of either the surfactant solution or the suspended precipitate particles in the medium (assumed to be the same) and L is the length of the porous solid. Pe^{-1} is the inverse of the pecllet number and represents the dispersion of the monomers. Pe is defined by:

$$Pe = \frac{u L}{D} \quad (8)$$

D is the dispersion coefficient.

Regular solution theory is utilized to describe the monomer-micelle equilibrium (18). For the SDS/DPC surfactant system, the following equations were used:

$$C_{m,ds} = X_{ds} CMC_{ds} \exp.\{ X_{dp}^2 w/RT \} \quad (9)$$

$$C_{m,dp} = X_{dp} CMC_{dp} \exp.\{ X_{ds}^2 w/RT \} \quad (10)$$

where w is the interaction parameter and X stands for the surfactant-based monomer mole fraction.

To obtain the Henry's law constants for the two surfactants, as shown in figures 4 and 5, the theoretical concentration history curves at the effluent and at various H 's were superimposed on the experimental breakthrough curves. The Henry's law constants

were chosen such that the tailing portion of the DPC and the leading part of the SDS match the experimental results. The rear part of the DPC and the front part of the SDS were chosen because these parts of the surfactant slugs are the one's that reach each other in-situ and interact to form precipitate. Since the medium is negatively charged in this study, the cationic surfactant, DPC, will have a much higher plateau adsorption and is thus injected first. While SDS, which has the same charge as the media surface, will be injected second. The Henry's law constant for DPC is found to be $3.0 \cdot 10^{-4}$, while for SDS it is $1.0 \cdot 10^{-4}$. The inability of the Trogus model to adequately predict the entire DPC and SDS concentration breakthrough curves within the limits of the experimental conditions used in this study is shown by the prediction of an early breakthrough of the front part or the premature desorption of the rear part of the surfactant slugs.

2.2.2 Phase Changes in Surfactant Solutions

Long range electrostatic interactions between cationic and anionic surfactants in an aqueous solution can lead to the formation of either precipitate or mixed micelles. The rates at which these two competing processes, micellinization and precipitation, take place are determined by the concentration and composition of the surfactants in the mixture. Amante has studied and obtained the entire precipitation region for the SDS/DPC surfactant system (19). Stellner, later, experimentally confirmed the reaction stoichiometry to be 1:1; that is, one mole of each surfactant is required to form one mole of precipitate (20). He also modeled the equilibrium phase boundaries for the cationic/anionic surfactant systems by accounting for the micellinization and precipitation. Stellner's model was used in this study to predict the equilibrium phase boundaries for the SDS/DPC system in the presence of 10% SFB solution. The 10% SFB is a dilution of a full strength synthetic field brine solution with a composition shown in table 1. Figure 6 is the representation of the theoretical model and the experimental results of the phase boundaries for this system.

Much of the precipitation work that has been done only dealt with the equilibrium conditions of precipitate and neglected consideration of the effect of supersaturation (21). In contrast, results from numerous studies confirm that many stoichiometric reactions are often slow and require long periods of time, even days, for completion of the reaction (2,22-24).

For the mechanisms of precipitation in surfactant solutions, three distinguishable steps are identified. The first criterion is that the monomer concentrations of surfactants must exceed the solubility product; following the development of the

solution turbidity (state of supersaturation), the second step consists of the appearance of stable minimum sized particles of precipitate (sometimes referred to as "nuclei") suspended in the bulk solution. The last step involves the growth of particles as molecules diffuse to the solid surface from the bulk solution. However, the ability of micellar aggregates to solubilize apolar substances, such as precipitates, prevents nucleation in regions beyond the phase boundaries. Such supersaturated mixtures only contribute to the growth of the particles and not to the nucleation; i.e., precipitation begins to form only when the solution concentrations fall within the phase boundaries of the surfactant systems.

The rate of nucleation is considered to be the principle physical phenomena in the precipitation process. The first nucleus that is formed in an aqueous environment requires n number of ionic compounds that constitute the solid crystal to combine together to produce the stable particles (25,26). In the case of SDS/DPC surfactant system, the equilibrium 1:1 reaction between the dodecylsulfate anion (DS^-) and dodecylpyridinium cation (Dp^+) may be written as:



where $(DsDp)_n$ represents the nucleus that is formed. If we limit ourselves to considering only primary homogeneous nucleation, which refers to the spontaneous formation of nuclei in the bulk of a supersaturated solution with or without the presence of any suspended crystals, then, the rate of nucleation, B° , can be described by an Arrhenius-type expression, (26-29):

$$B^\circ = c \exp.\{-\Delta G^*/KT\} \quad (12)$$

where B° is the number of particles produced per cm^3 per second, ΔG^* is the activation energy or the energy barrier that solute clusters have to overcome before a nucleus is produced, K is the Boltzmann's constant, T is the absolute temperature, and the pre-exponential factor c is estimated to have a value of 10^{25} to 10^{30} (26,27). The above equation has been used with some success in numerous studies since it was first proposed by Volmer and Weber back in 1926 (26,30). The local energy fluctuations caused by changes in some characteristics of the system such as concentration or relative supersaturation among others, allow some solute clusters to gain sufficient energy to overcome the energy barrier, ΔG^* . This driving force allows the process to proceed in the direction of a decrease in the free energy of the system and to relieve the level of supersaturation by producing some nuclei. The energy barrier is the lump sum of the energies required to form an interface with a specific surface energy (τ), and the energy required to transform the solute clusters from liquid crystalline state into solid crystalline state (27).

From these thermodynamic conditions necessary to have a homogeneous nucleation, G^* can be estimated to be (26,27):

$$\Delta G^* = \frac{\beta (\tau)^3 v^2}{\theta^2} \quad (13)$$

where β is a shape factor and can be expressed as (26):

$$\beta = \frac{4 A^3}{27 v^2} \quad (14)$$

A is the surface area, v is the molecular volume of the nucleus, and θ is the difference between the chemical potentials of a solute in the crystalline state and in solution expressed by Gibbs-Thompson equation as (26,27):

$$\theta = K T \ln(rs) \quad (15)$$

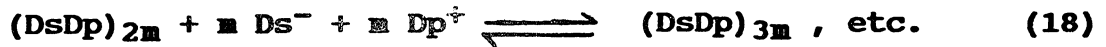
If equations (12) through (15) are combined together, the rate of nucleation can be expressed in terms of the relative supersaturation (rs) by:

$$B^{\circ} = c \exp. \left\{ - \frac{\beta (\tau)^3 v^2}{K^3 T^3 (\ln rs)^2} \right\} \quad (16)$$

The second step in the formation of a solid precipitate involves the growth of particles already present in the solution. In the precipitation of ionic salts from solution, the addition of individual ions to the surface of the solid crystal is the main reason for the growth. Two distinct steps are involved in the growth process. In the first step, the diffusion mechanisms allow the transport of the molecules from the bulk supersaturated solution to the crystal surface. In the case of SDS/DPC surfactant system (where there is a one to one stoichiometric ratio between the two surfactants constituting the solid precipitate), to maintain the stoichiometric proportions and to hold the condition of electroneutrality of the particles, there must be an equal net flux of the two oppositely charged surfactant monomers to the surface of the solid crystal. In the second step, surface reaction mechanisms (in the system studied here, nucleation reactions at the surface) take place which allow the solute molecules to orient and incorporate into the lattice structure of the crystals. The rate limiting step for the growth process can be assumed to be the diffusion step if the interfacial reactions happen so fast that the equilibrium at the interface is rapidly reached. It can be assumed that the diffusion-controlled growth mechanism is a realistic assumption in the light of the facts that the flow of fluids through the porous medium is assumed to be laminar under

the conditions inhabited in the injection processes, and also that nucleation occurs so fast at the solid surface.

The mechanism of crystal growth for the SDS/DPC surfactant system can be represented as follows:



The rate of growth can be expressed to a good approximation and in fairly large intervals of relative supersaturation by (26):

$$\frac{dM}{dt} = k / a_{p,b} (rs) \quad (19)$$

where $a_{p,b}$ is the specific surface area of the particles in the bulk solution, and $k/$ is the mass transfer coefficient and is estimated by correlations for forced convection around suspended particles. The specific surface area was calculated by dividing the total mass concentration of suspended particles by the mass of one particle and multiplied by the surface area of one particle having an average characteristic dimension. It was also assumed that the precipitation is highly monodisperse and that the individual particles have both the same shape and size. Under these conditions the growth rate is the same for all particles.

Diffusion is also believed to be the rate determining factor in most cases of dissolution (26). In this study the dissolution process is treated as the growth process although with a negative relative supersaturation. The rate of dissolution is thus negative.

Certain conditions have been established here to distinguish between growth and dissolution. The suspended particles undergo growth if the surrounding solution contains an excess of both surfactant monomers and also that the solution has a relative supersaturation greater than zero. This criterion places the solution concentrations above the solubility line; however, if the fluid that is streaming by, bringing fresh solution to the surface of the particle, does not possess both surfactant monomers, it would promote the dissolution.

The fundamental mass transfer driving force for precipitation has been shown in this study to be the relative supersaturation (rs). Let's define supersaturation, s , by:

$$s = C_{m,dp} C_{m,ds} - (C_{dp})^* (C_{ds})^* \quad (20)$$

where the first term is the product of concentrations of cationic and anionic surfactant monomers in solution and the second term is the product of the surface concentrations. When the interfacial reaction is fast, surface concentrations are equal to the equilibrium concentrations and their product can be represented by the solubility product (K_{sp}/f^2). The relative supersaturation, r_s , can then be defined as:

$$r_s = \frac{C_{m,dp} C_{m,ds}}{K_{sp}/f^2} - 1.0 \quad (21)$$

Therefore r_s is a measure that determines how far the solution is from the equilibrium condition. Figure 7 represents different levels of r_s 's as parallel lines to the equilibrium line, superimposed on the SDS/DPC phase diagram. The farther these lines are from the K_{sp} line, the better the chance there is to form a colloidal suspension with a very large number of small particles in very short time intervals; i.e., nucleation is dominant at very high r_s 's. However, in regions close to the equilibrium line (sometimes referred to as "metastable region"), the growth process is dominant (21). Figure 8 shows the rates of nucleation and crystal growth as functions of r_s . The critical relative supersaturation (r_{sc}) is defined to be the r_s at which the rate of nucleation is equal to the rate of particle growth. For solutions with r_s less than r_{sc} , precipitation is slow and follows the growth mechanism. For solutions with r_s greater than r_{sc} , the precipitation is fast and many nuclei form. The r_{sc} for the system studied in this work was calculated to be around 50.

2.2.3 Variations of Permeability with Surfactant Precipitation

As the surfactant solutions flow through the homogeneous porous medium and interact to form precipitate, these generated suspended, solid particles with sizes smaller than the pores of the medium may be retained on the mineral surface. The deposited particles may also come off the pore walls at a later time, and then be transported with the fluid flow until they reach another retention site and are deposited either on the surface of the medium or on the layer of particles already covering the surface. As the mass concentration of the deposited particles reaches the capacity of the surface (σ_t), the porous medium becomes less retaining due to the lack of sufficient retention sites; thus, a maximum state of permeability reduction is reached at this point. One overall objective of this research topic is to evaluate the effects that deposited particles have on local permeability.

The process of precipitation in porous media and particle

retention, in some respects, is analogous to the process of deep-bed filtration which is implemented to investigate the removal of suspended matter from fluids and has been researched for so many years (33). The work of numerous investigators on classification and elementary mechanisms of different sized particles has been reviewed by Herzig et al (34). It has been suggested, in several studies, that for particles less than 3μ in diameter (particles involved in this research), the plugging process occurs by physicochemical means with surface sites as the locations the deposited particles occupy. Other retention sites, such as crevice sites, constriction sites, or cavern sites are not expected to be the potential sites for deposition of these particles. The mechanisms of attachment is believed to be dependent on surface forces such as Van der Waals, electrokinetic, and electrostatic forces (10,34). Direct interception is expected to be the main reason bringing the particles to the surface of the medium (34). Sedimentation and diffusion effects are negligible for such small particles.

Mass balance equations and kinetic equations describing the rate of retention and entrainment of particles are used in this study to mathematically describe the plugging of a porous medium. The conservation equation for the precipitate particles may be written as:

$$\frac{dM}{dt} = -u \frac{dM}{dx} + \left[\frac{dM}{dt} \right]_{gen} \quad (22)$$

The generation term, $[\partial M/\partial t]_{gen}$, is the lump sum of the rates of nucleation and crystal growth,

$$\left[\frac{dM}{dt} \right]_{gen} = B^{\circ} v^{\circ} \rho_p + k/ a_{p,b} (rs) \quad (23)$$

where ρ_p is particle density, and M is the total mass concentration of precipitate and is shown by:

$$M = \phi c_p + \sigma \quad (24)$$

where ϕ is the porosity, c_p is the mass concentration of suspended particles and σ is the mass concentration of deposited particles. Moreover, if only the suspended particles are allowed to move, substitution of equations (23), (24), (6), and (7) into the mass balance equation (22) gives:

$$\frac{d}{dt} [\phi c_p + \sigma] = - \frac{d}{dx} [\phi c_p] + [B^{\circ} v^{\circ} \rho_p + k/ a_{p,b} (rs)] \quad (25)$$

The kinetic equation for the two directional exchange of particles, namely, the processes of retention and entrainment, is developed by considering the maximum capacity of available surface sites for deposition, the fluid shear forces on the retained particles, and the experimentally determined first order dependence of the rate of retention on mass concentration of particles in the bulk solution and of the rate of entrainment on mass concentration of particles on the surface. (35). The net rate of particle deposition on the surface of the medium is shown as:

$$\frac{d\sigma}{dt} = k_1 u c_p (\sigma_t - \sigma) + k_2 \sigma \frac{dp}{dx} \quad (26)$$

where k_1 and k_2 are the coefficients of retention and entrainment respectively, and dp/dx is the differential pressure in the direction of flow and is shown by Darcy's law to be inversely proportional to permeability, k .

$$\frac{dp}{dx} = -u \frac{\mu}{k} \quad (27)$$

There have been numerous attempts to use modified versions of the original Kozeny-Carman equation in order to relate the mass concentration of deposited materials to the pressure drop of the fluid across a plugged media (34) but, in most of these cases, the changes in pressure drop were too small and only a qualitative description of the actual process could be achieved (34,36). The Kozeny model, however, was used successively for a clean porous medium with very fine particles (38,39). To magnify the effects of σ on changes in pressure drop or permeability, empirical models were used (35,39,40). The development of the following empirical relationship between permeability and mass concentration of retained precipitate, used in this study, is shown in Appendix A:

$$\frac{k}{k_0} = \frac{[1 - (\sigma/\sigma_t)^n]^3}{[1 + (\phi_0/1-\phi_0) (\sigma/\sigma_t)^n]^2} \quad (28)$$

where ϕ_0 is the initial porosity, σ_t is the maximum capacity of the media for purpose of the particle retention, and n is an empirical constant.

An explicit backward finite difference method is used to numerically solve for C_{ds} , C_{dp} , σ , c_p , M , ϕ , k for successive time steps.

2.3 MODEL VALIDATION BY COMPARISONS BETWEEN THEORETICAL AND EXPERIMENTAL RESULTS

It is now possible to demonstrate how the analysis can be used with the appropriate experimental parameters to show its validity in correlating the experimental data. However, several parameters do need to be identified before comparing the theoretical results with those obtained from experiments.

One-dimensional transport of solute in a saturated porous medium has been simulated by assuming that the first precipitate particle is spherical in shape with a molecular volume to be determined by dividing the molecular weight of the nucleus by the density of the particle and by the Avogadro's number. The radius of the nucleus particle is then the cube root of the molecular volume. Furthermore, since it is a general belief that much of the mass transfer occurs due to crystal growth and not nucleation (36), we assume that the average size of the growing particles is one order of magnitude larger than the nucleus. No secondary nucleation, which requires the presence of solute crystals, will be considered in this model. Coprecipitation mainly due to nucleation near the surface of the solid particle is the reason for particle growth. Molecular diffusion coefficients for all components are assumed to be equal. The solid particle is assumed to be nonporous and does not contain any liquid in itself. The growing crystals move through the porous medium at the same speed as the flowing medium. The deposited particles are transported through the medium only when they are first entrained to the surrounding liquid; that is, no leap frogging of the deposited particles on the solid surface is allowed. Finally, as the last constraint on the model, the straining action of the precipitate particles, which could result in the blockage of the pore throats, is prevented by choosing the size of the suspended particles to be about two orders of magnitude smaller than the mean pore size. The numerical values of the parameters used in this model are listed in table 2.

Three experiments were chosen from the previous studies on surfactant precipitation in porous media to be compared with the results obtained from the theoretical model presented in this paper. The conditions considered for the comparison studies are shown in table 3. Figures 9 through 11 present concentration history curves for DPC surfactant and suspended precipitate at the outlet end of the porous solid.

The early breakthrough for the theoretically computed concentration is expected because the adsorption model used in this study, the Trogus model, was incapable of predicting the entire surfactant concentration history curve (refer to figure

4). Only the rear part of the DPC was matched to the experimental results. Moreover, as expected, following injection of brine, a decrease in DPC concentration is computed; however, upon injection of the second surfactant, SDS, a sharp increase in DPC concentration is obtained. This increase, which in some cases exceeds the injected concentration, is believed to be due to a faster desorption of DPC from the solid surface by the SDS surfactant slug front. Desorption of an adsorbed component was shown in other studies to be faster when the porous medium is injected with a less adsorbing component than with a non-adsorbing component (17,41,42). After a momentary increase, the effluent DPC concentration decreases fairly rapidly. Moreover, since it is assumed that the precipitation only occurs in the bulk solution, the precipitation at the solid surface between the anionic surfactant monomer and the cationic surfactant admicelle is not considered and is neglected. In real situations, once the first surfactant is desorbed from the surface, it may be caught up and interact with the incoming second surfactant before it is a freely dispersed monomer. The mechanism by which precipitation occurs near the surface is different from that which occurs in the bulk solution. This seems to be a possible explanation for the sharp increase in the theoretical DPC concentration. This increase is not perceived in the actual tests because precipitation is allowed everywhere including on the solid surface. Precipitation was also observed at a time later than what the model predicts. This is because of the fact that in the early stages of the precipitation, particles are so small to be seen by naked eye, it is possible that the operator was not aware of the presence of precipitate in solutions and thus a higher concentration was measured for the solutions. The model also did not show the appearance of any precipitate at the effluent solution at the time at which particles of precipitate were detected visually.

Figures 12 through 14 show the experimental and theoretical average permeabilities for the two halves of the porous solid media as a function of pore volumes injected. As can be seen from the plots, there is a qualitative agreement between the theoretically computed formation permeabilities and the actual measured permeabilities. There are two possibilities for the disagreement that exists between the experimental values of permeabilities at the outlet section and those predicted by the currently proposed theoretical model. As mentioned before, the Trogus model does not precisely predict the surfactant adsorption isotherms under the conditions cited in this study. Furthermore, the precipitate particles may propagate at a lower velocity than the bulk fluid velocity assumed in this work. Another similarity between the theoretical and experimental work is the slow recovery of the permeabilities as injection of brine solution continues.

The model is also capable of monitoring the location at which the suspended and deposited precipitates are present at any time. Figures 15 through 17 show the precipitate profiles at different pore volumes injected. While the surfactant slugs do spread along the length of the media and mix with each other to form new precipitate particles, the suspended particles move through the medium at the bulk fluid velocity. It is apparent from the plots that a limited size for the second surfactant solution is required in order to deposit a certain amount of precipitate and to reduce the permeability. Any further injection of this solution will not contribute to formation of more precipitate, as the first surfactant is consumed during the precipitation process or is simply eluted from the media.

2.4 CONCLUSIONS

The most important feature of this simulation is that it is possible to use pure component adsorption isotherms, mixture phase diagrams, and experimentally determined kinetic rate constants as input to the model to predict the differential permeability reductions at every stage of the process. The empirical relationship developed to correlate the permeability reductions as function of mass concentration of precipitate predicts, at least qualitatively, the trends at which the observed in the experimental results. The use of an adjustable parameter for magnifying the effect of deposited precipitate on local permeabilities suggests that the permeability reductions are achieved not only by the accumulation of precipitate on the solid surface, which eventually reduces the space available for flow to go through, but also by blocking the pore throats by, for example, a straining action.

This work also establishes other factors such as plug location, time to onset of plugging, and determination of how dilute the surfactant solutions may be made, as a function of permeability. Optimization studies are presented elsewhere (43). Overall, the present model contributes to a better prediction of permeability variations caused by precipitation of surfactant solutions in a porous medium. Several parameters, especially the rate constants which have been assumed in this work, should be thoroughly investigated before the proposed model is to be extended to include reservoir heterogeneity, two dimensional flow, and oil mobilization.

Table 1
Synthetic Field Brine (SFB) composition

component	Kg/m³
NaCl	12.31
CaCl₂	0.32
MgCl₂.6H₂O	0.44
NH₄Cl	0.07
Na₂B₄O₇.10H₂O	0.34

Table 2

Characteristics of solid precipitate and SDS/DPC surfactant system

SOLID PRECIPITATE

ρ_p	= 2.0 g/cm ³ *
τ	= 27 ergs/cm ² *
V	= 4.525 * 10 ⁻²² cm ³ *
k_1	= 5.0 cm ² /g *
k_2	= 1.0 * 10 ⁻¹⁰ cm ² sec/g *
d_{nuclei}	= 1.5 * 10 ⁻⁷ cm
d_p	= 1.5 * 10 ⁻⁶ cm
K_{sp}	= 115 μ M ² @ T = 25°C
w/RT	= - 8.62
β	= 16 $\pi/3$ (for spheres)
c	= 1 * 10 ³⁰
n	= 0.25 *
α	= 10.0 ‡
m	= 1 *

SDS/DPC surfactant system

CMC_{ds}	= 1650 μ M	T	= 25°C
CMC_{dp}	= 7500 μ M	μ	= 1 cp
H_{ds}	= 1 * 10 ⁻⁴ , l/g	ρ_s	= 2.75 g/cm ³
H_{dp}	= 3 * 10 ⁻⁴ , l/g		

Porous media : Berea sandstone core

* data assumed in this study

‡ Herzig et al

Table 3

Conditions for the experimental and theoretical work

	run # 1	run # 2	run # 3
edp (pv)	11.24	9.96	9.50
eb (pv)	0.22	0.68	0.58
eds (pv)	4.76	3.54	4.46
d _{pin} (μM)	15000	15000	15000
d _{sin} (μM)	7000	6000	7000
k _o (md)			
inlet	156.2	46.1	159.4
outlet	224.8	116.0	230.0
u (cm/sec)	0.0025	0.0025	0.0027
φ _o	0.221	0.239	0.2125
L (cm)	14.40	16.55	16.55

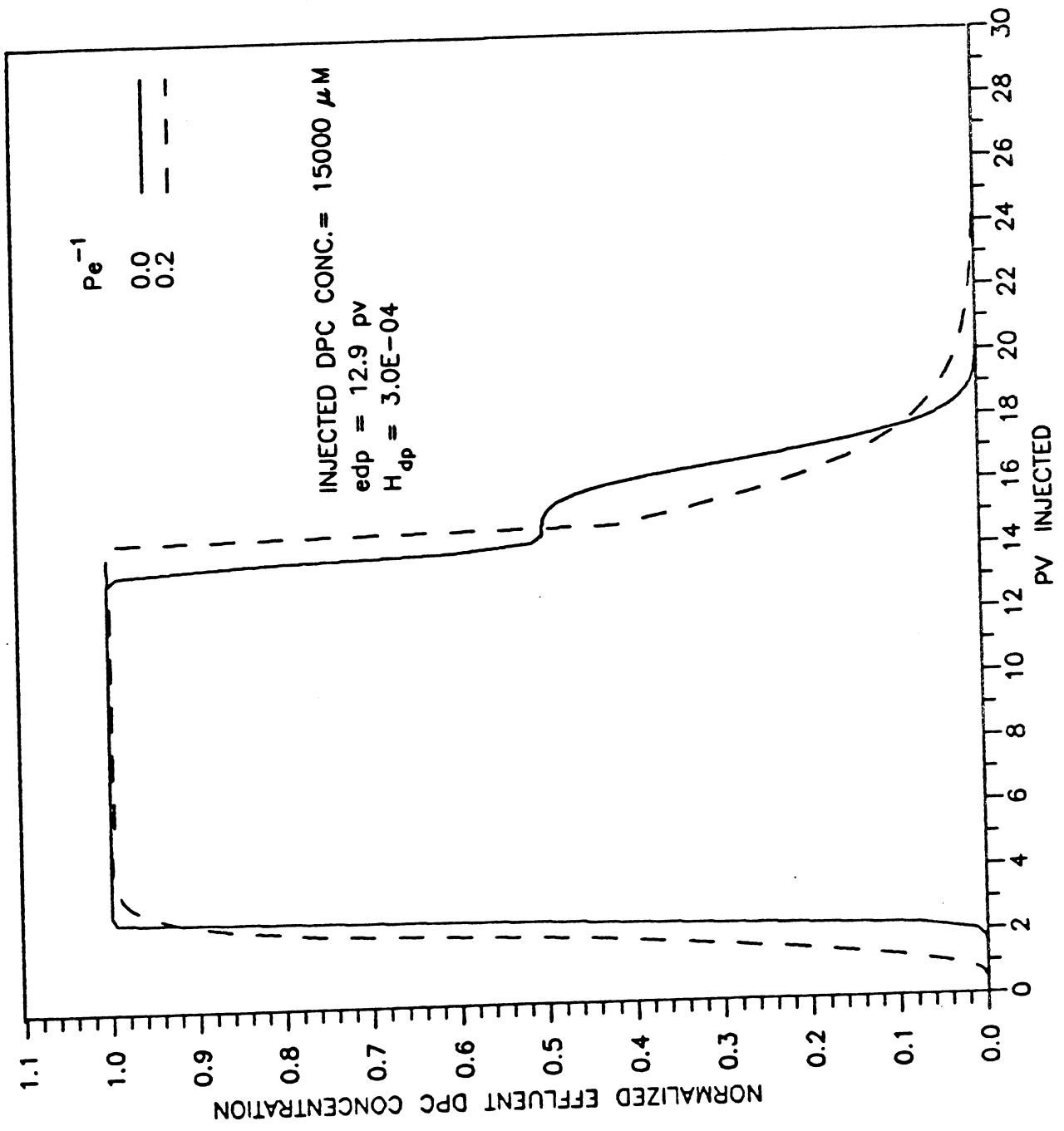


Figure 1 -- Effect of dispersion on typical breakthrough curves

Surfactant	Structure
Sodium Dodecyl Sulfate	$\text{H}_3\text{C}-(\text{CH}_2)_{11}-\text{O}-\text{S}(=\text{O})_2-\text{O}^- \text{Na}^+$
Dodecyl Pyridinium Chloride	$\text{H}_3\text{C}-(\text{CH}_2)_{11}-\text{N}^+\text{C}_5\text{H}_4\text{Cl}^-$ 

Figure 2 - Chemical structure of surfactants used in the experimental work

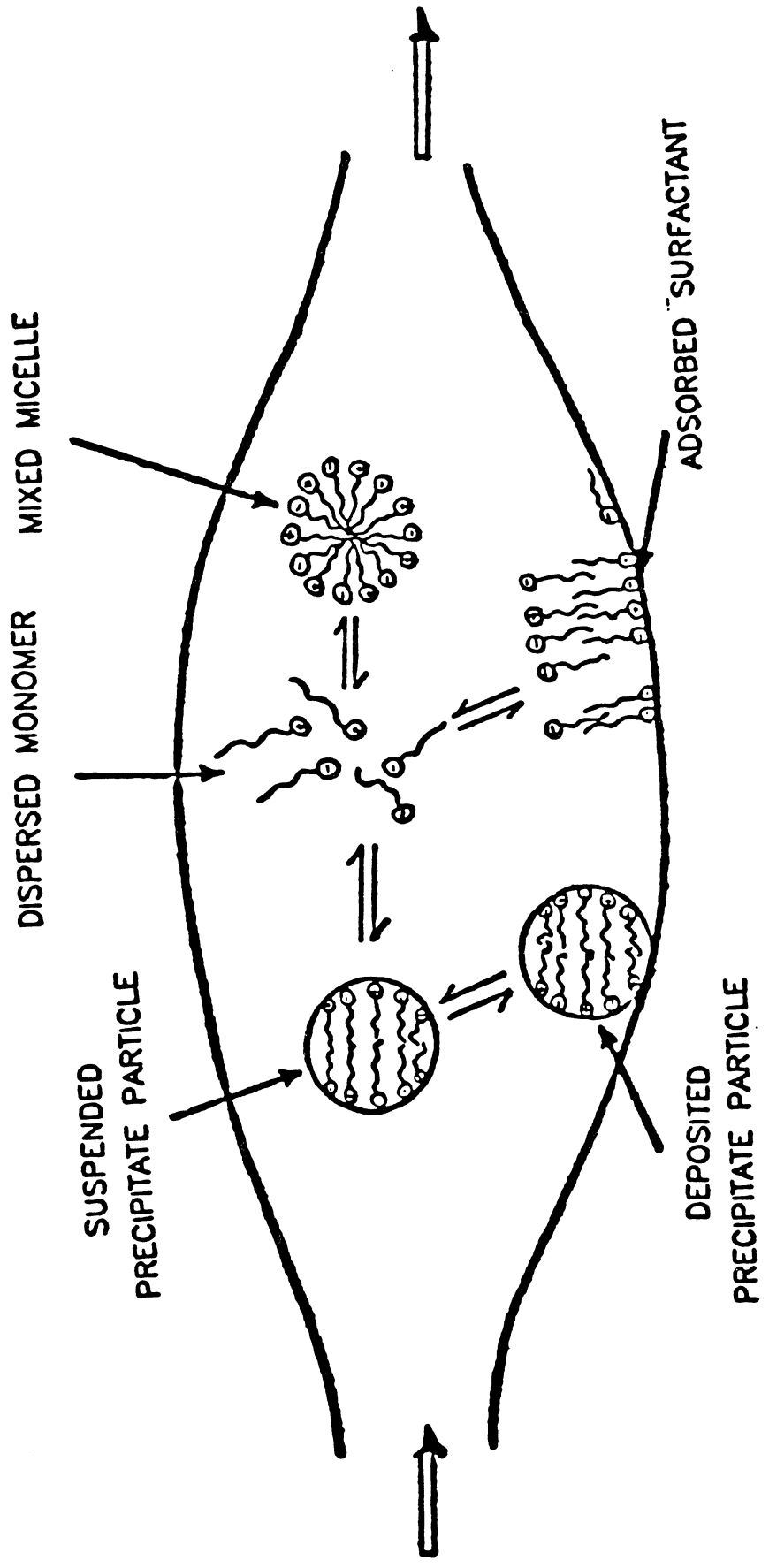


Figure 3 - Schematic representation of the equilibrium conditions for an anionic-cationic surfactant system in a porous media

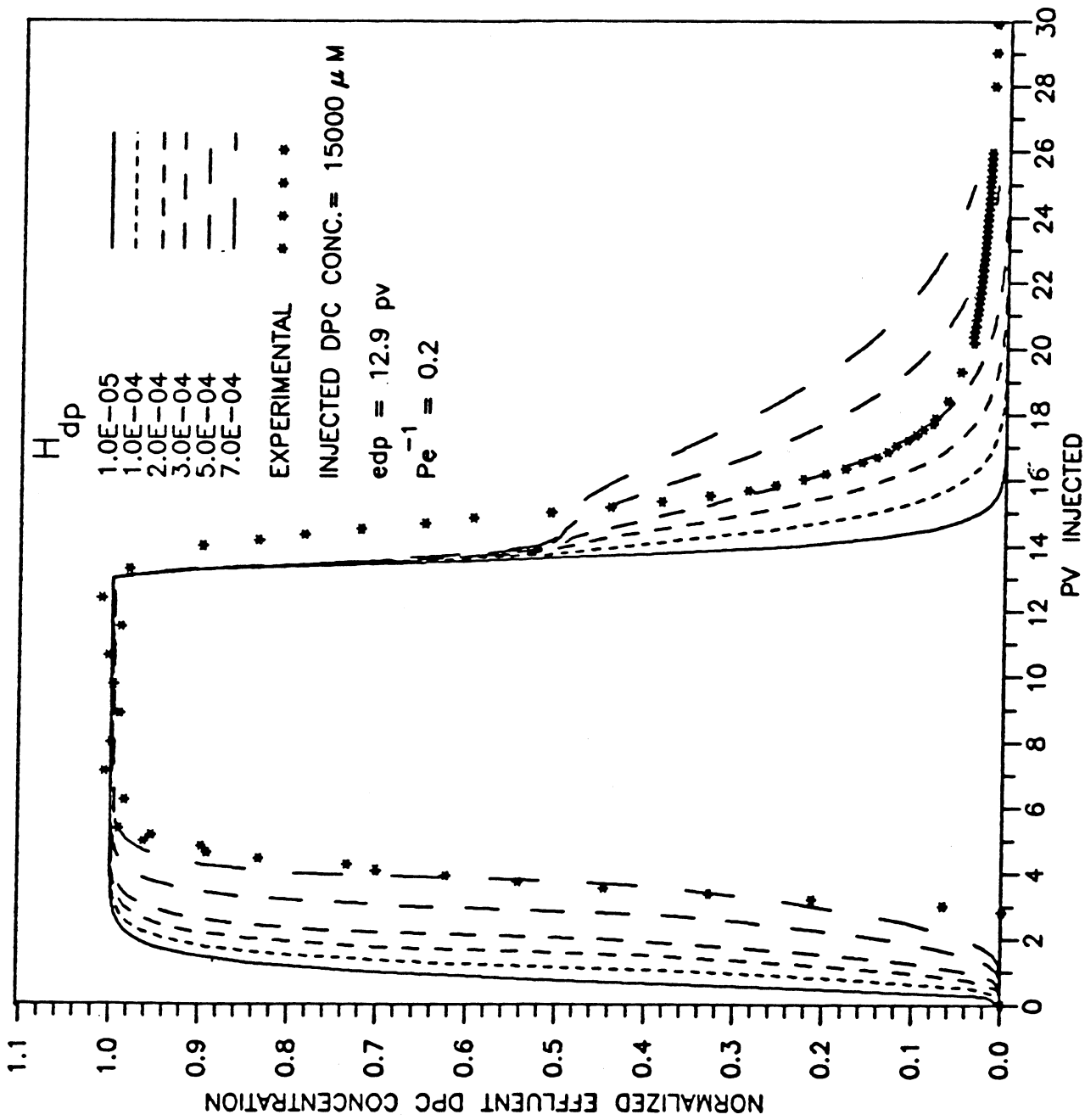


Figure 4 - Theoretical and experimental breakthrough curves for DPC

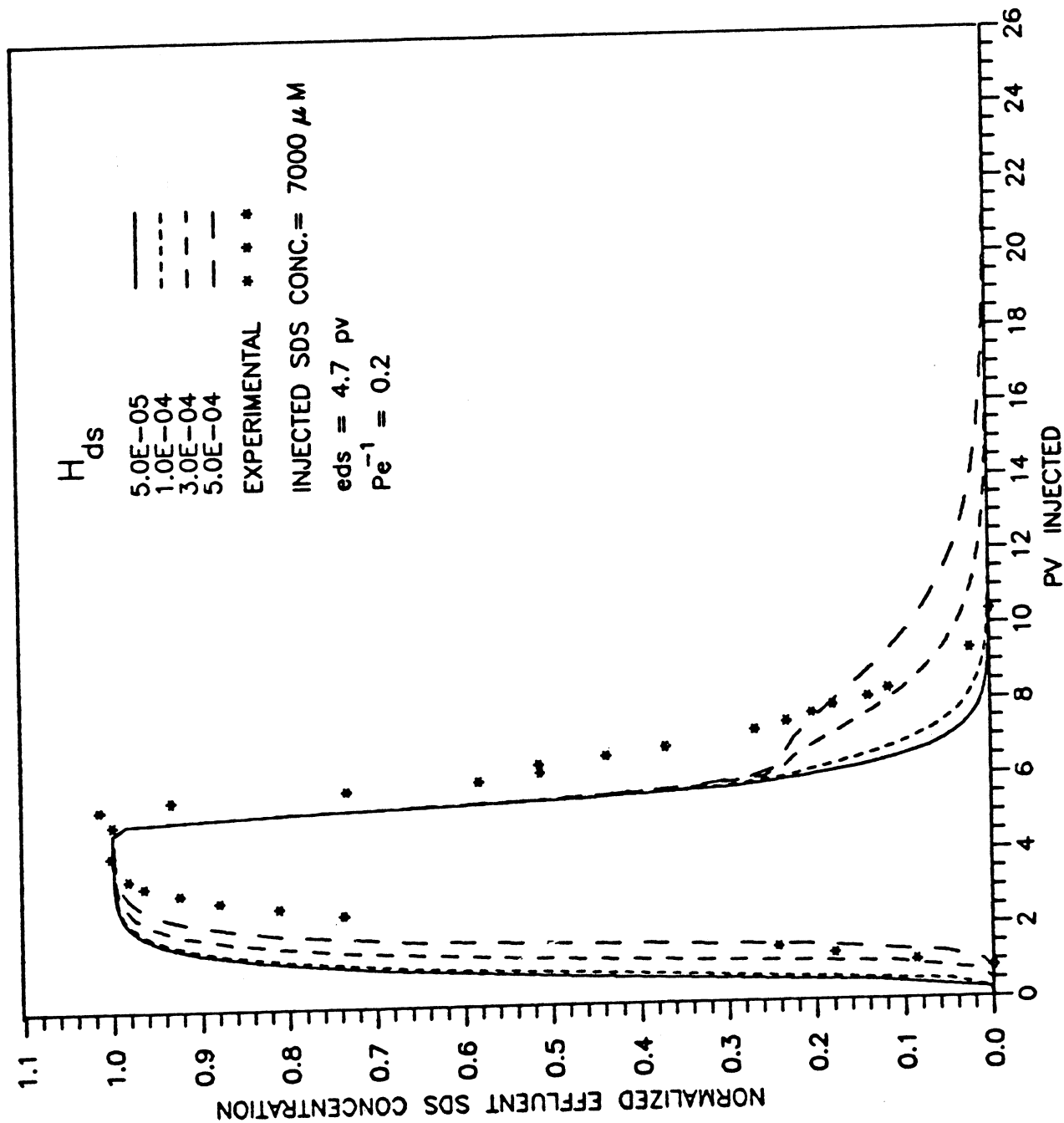


Figure 5 -- Theoretical and experimental breakthrough curves for SDS

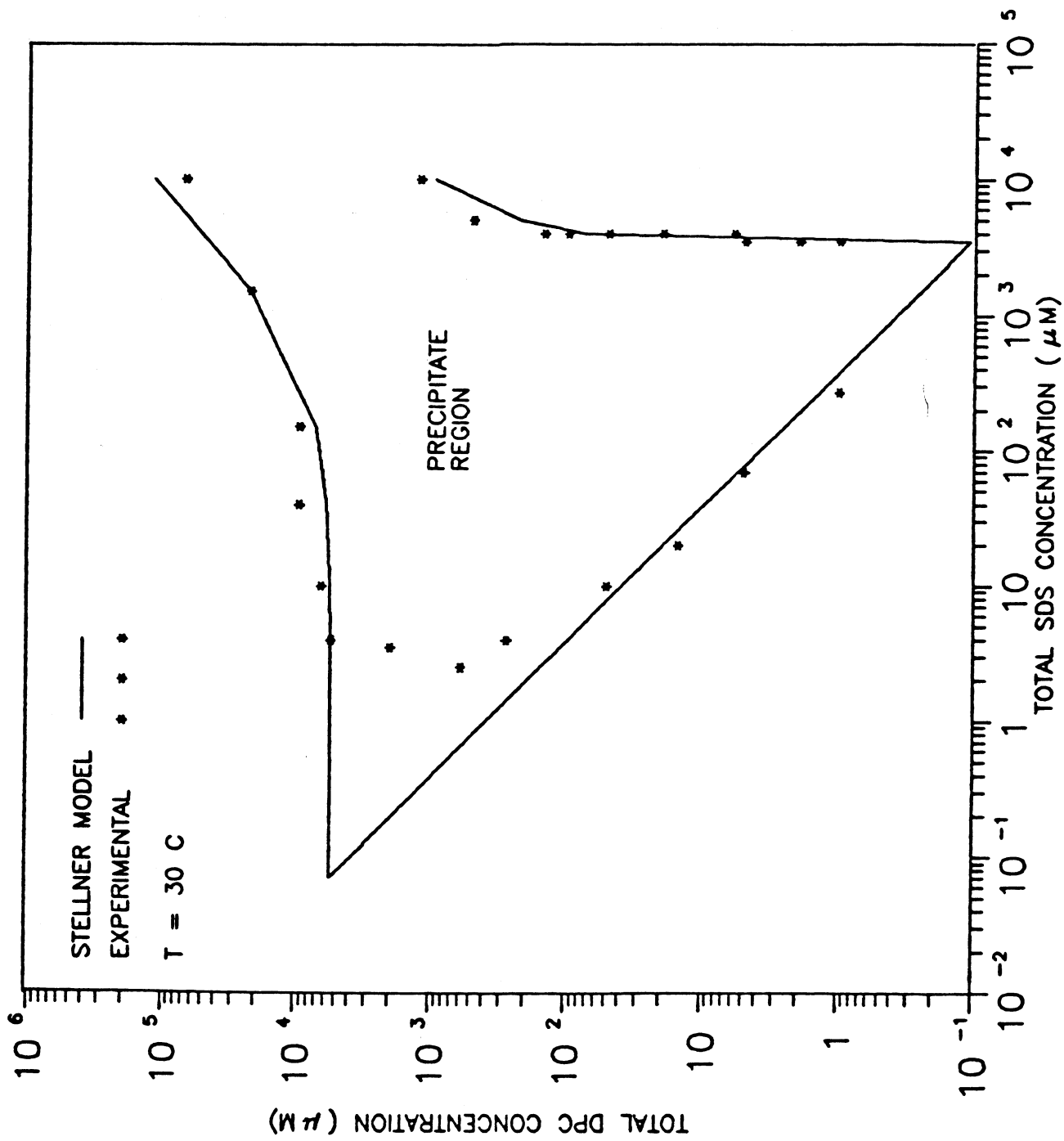


Figure 6 - Phase diagram for the SDS/DPC surfactant system

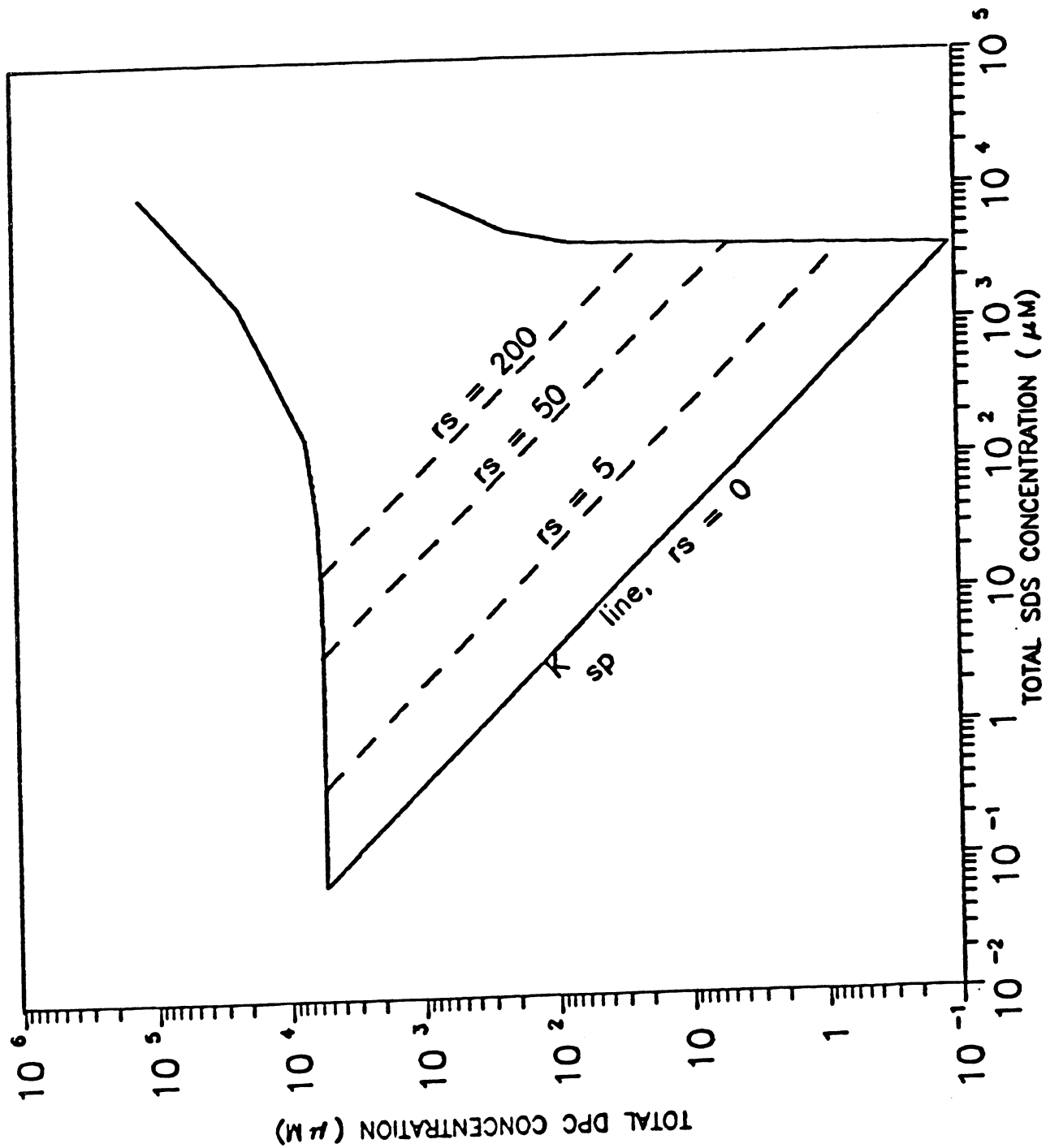


Figure 7 - Lines of r_s superimposed on SDS/DPC phase diagram

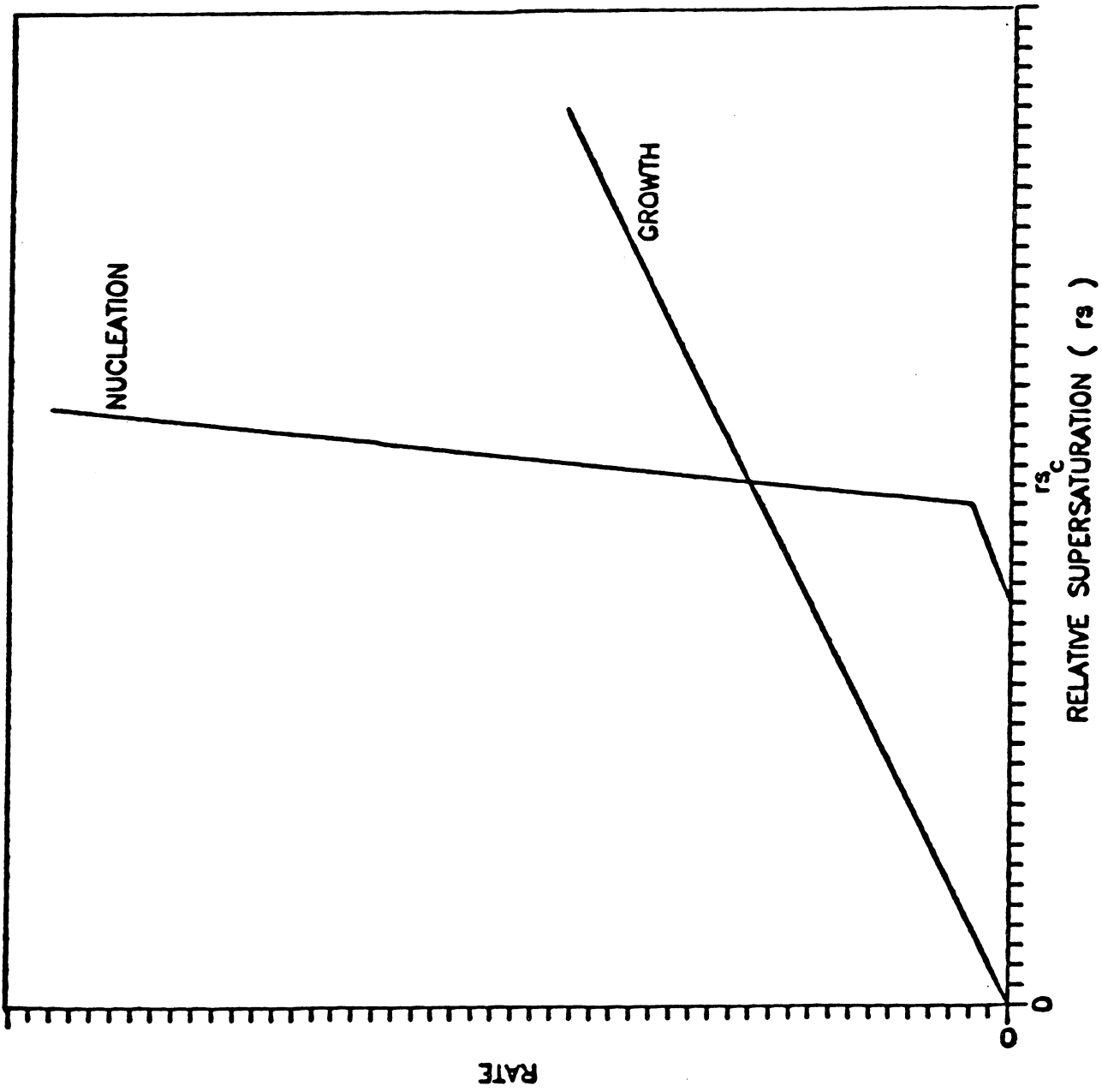


Figure 8 - Rates of nucleation and growth

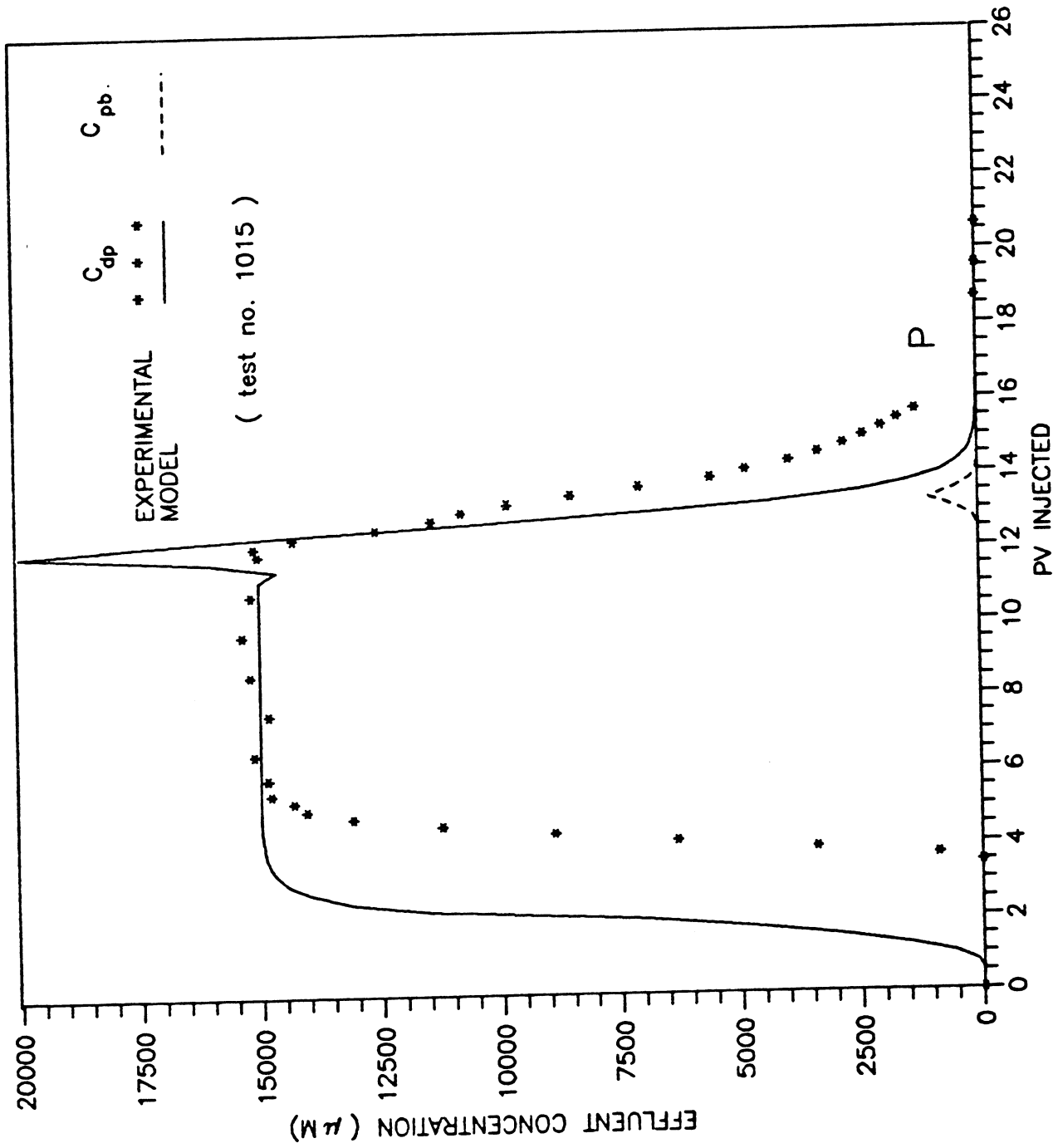


Figure 9 - Concentration history curves, run # 1

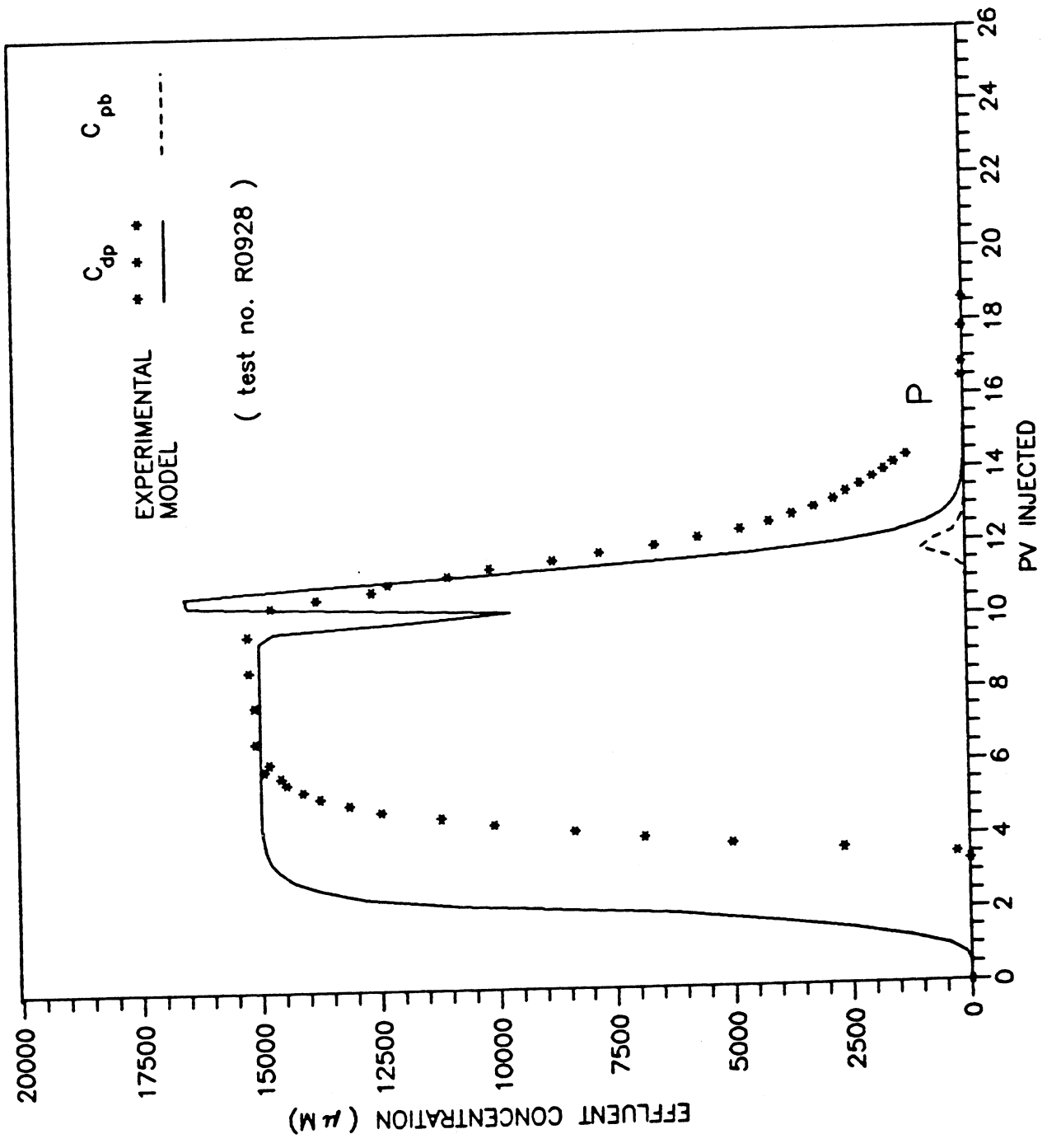


Figure 11 - Concentration history curves, run # 3

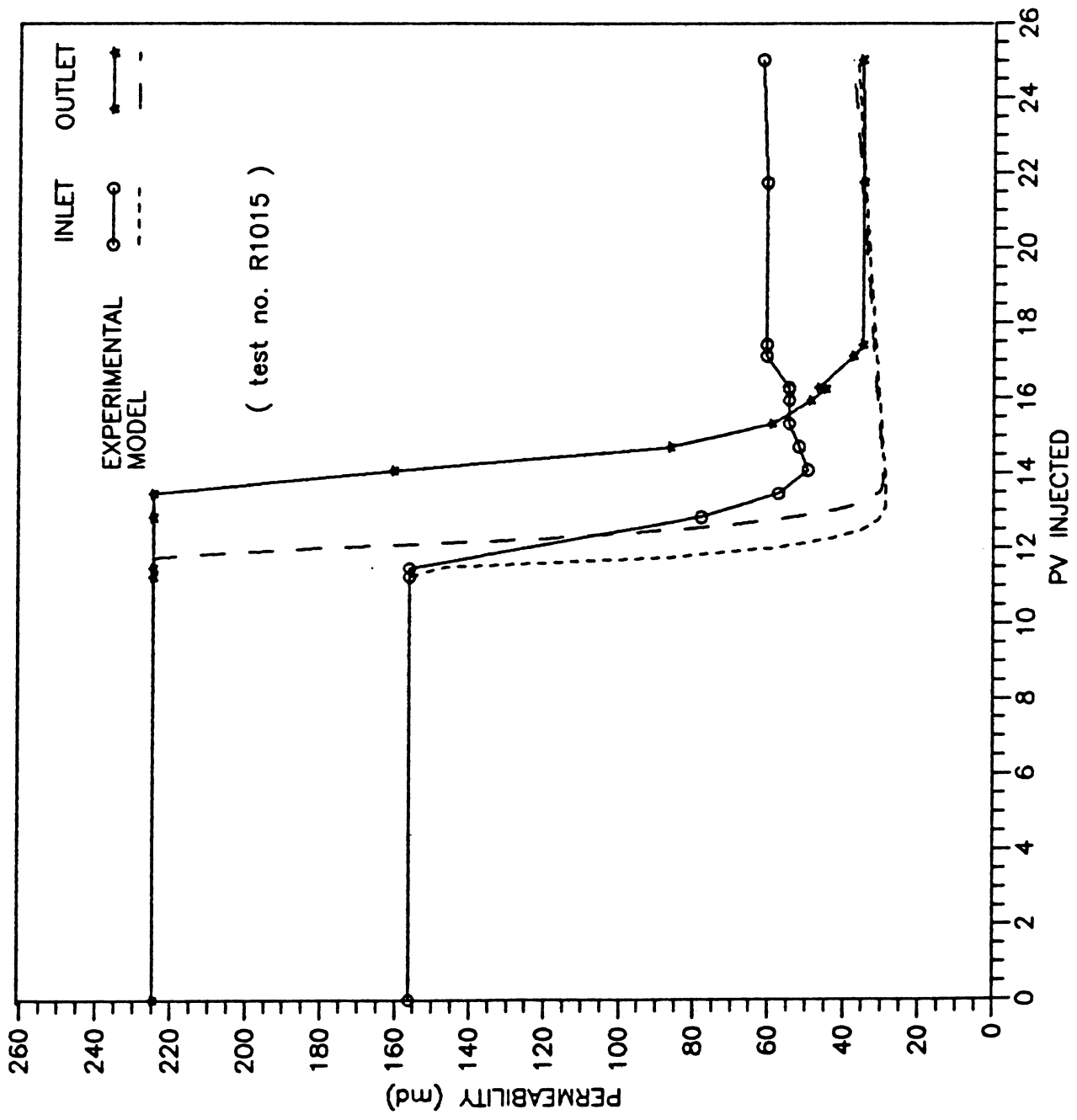


Figure 12 - Permeability vs. pore volumes injected, run # 1

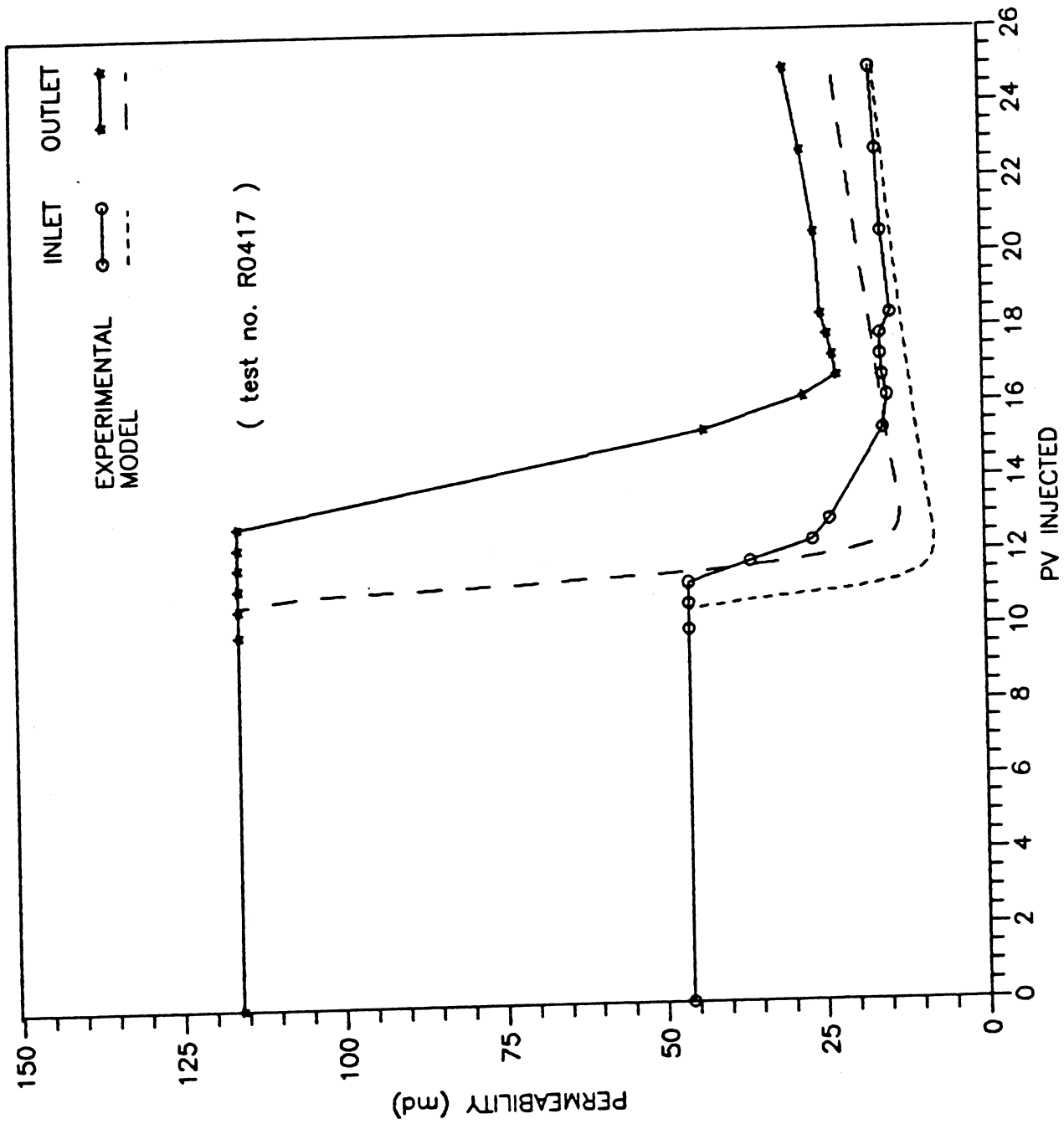


Figure 13 - Permeability vs. pore volumes injected, run # 2

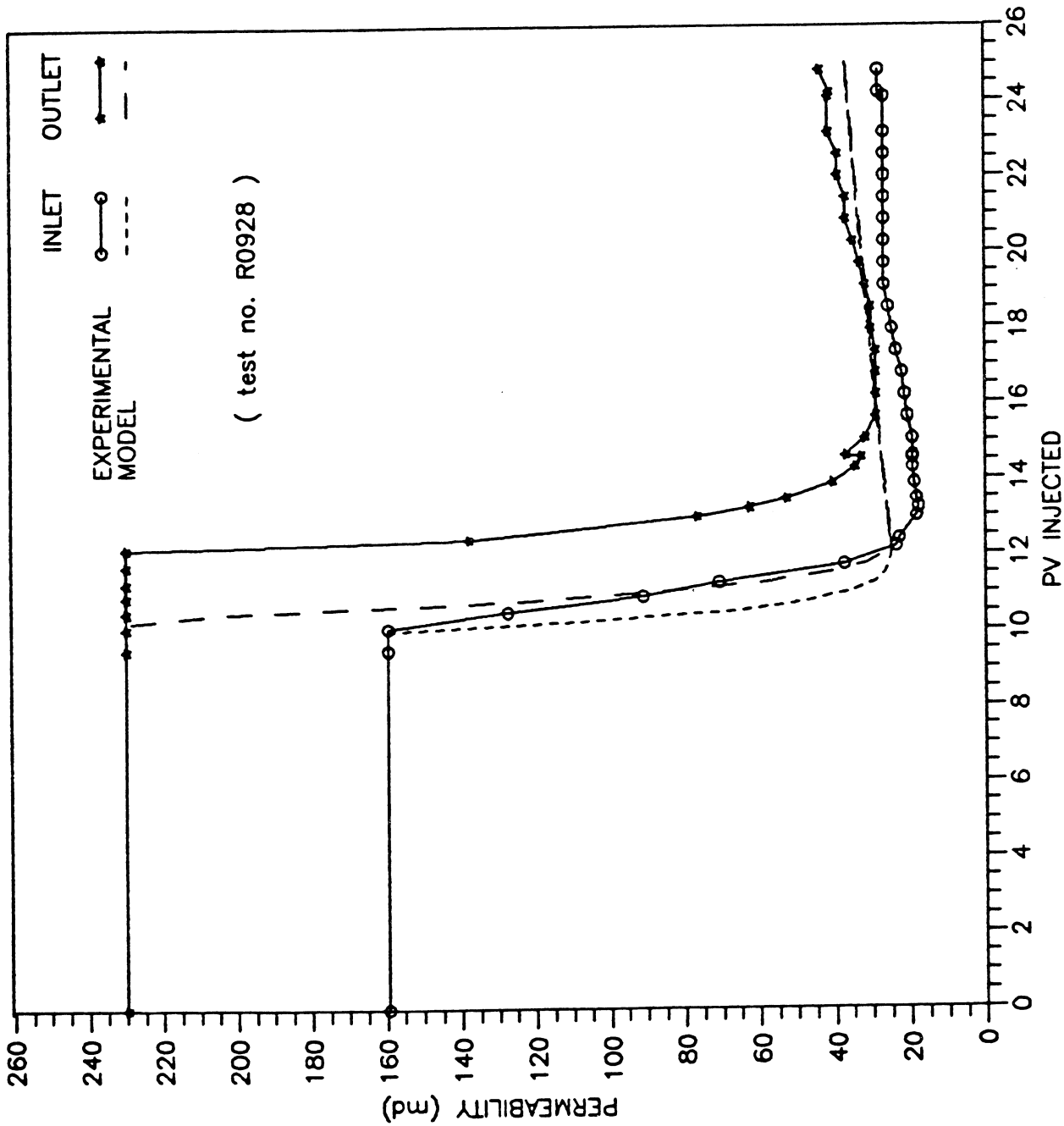


Figure 14 - Permeability vs. pore volumes injected, run # 3

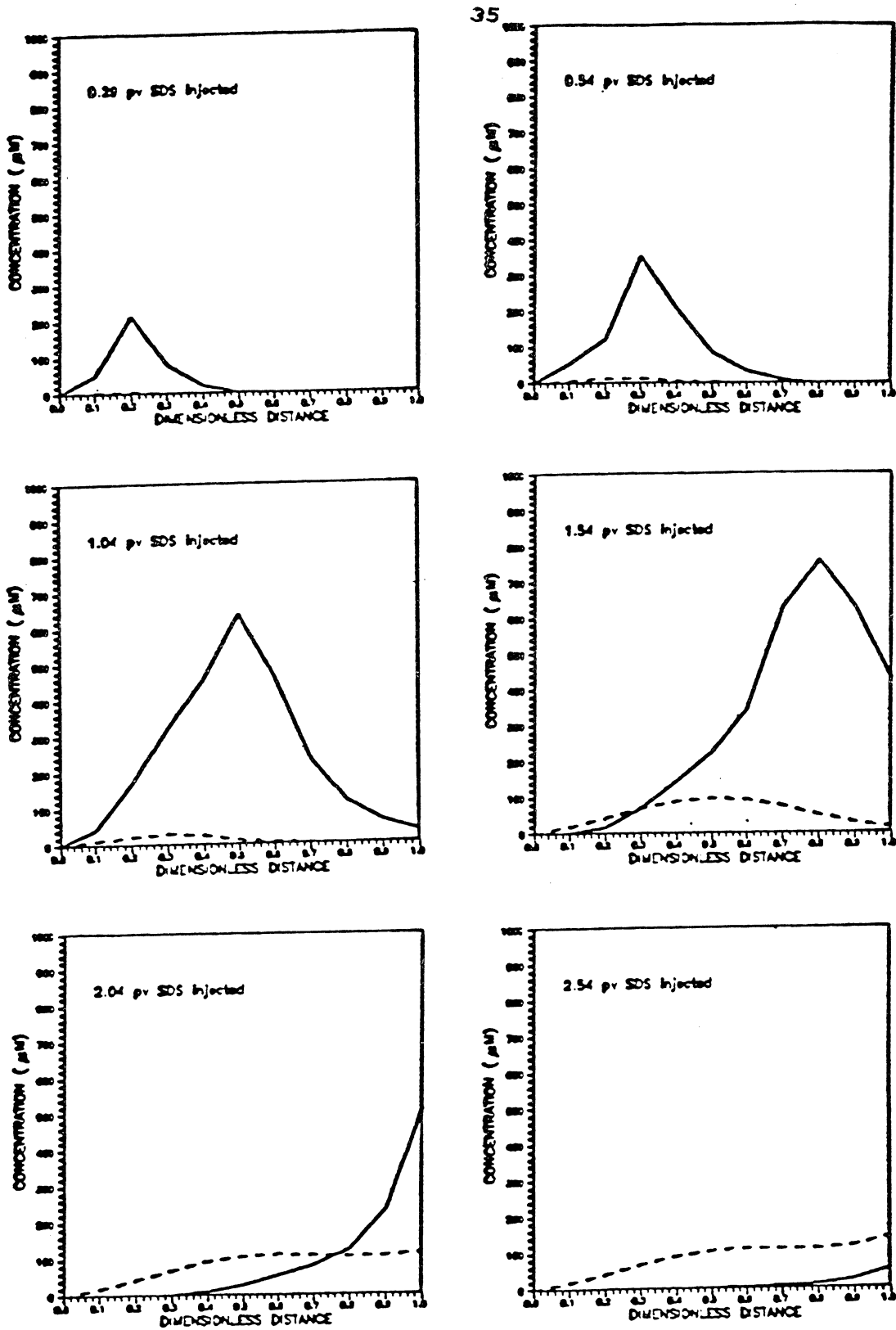


Figure 15 - Precipitate profiles, run # 1

solid lines represent molar concentration of suspended precipitate
dashed lines represent molar concentration of deposited precipitate

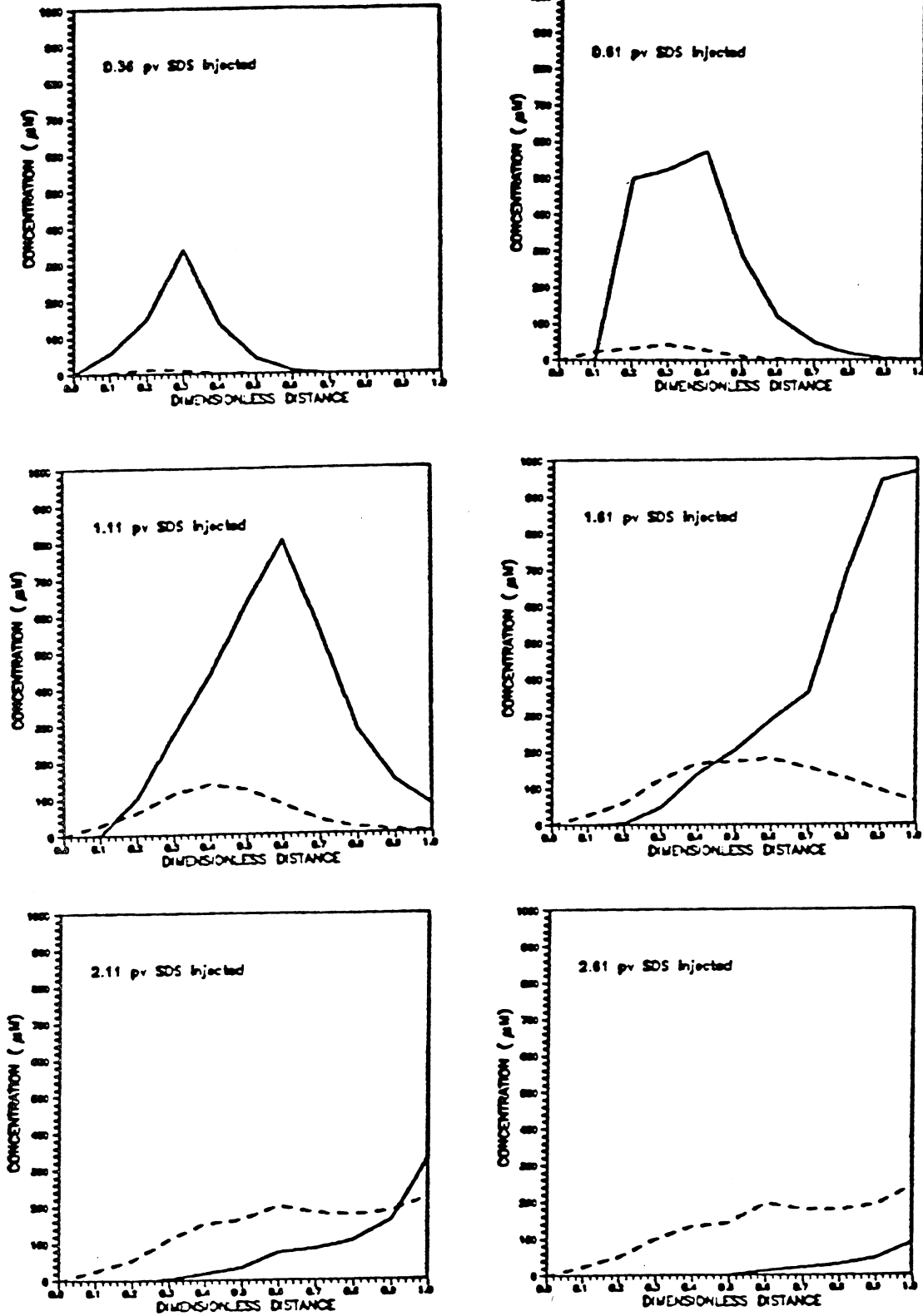


Figure 16 – precipitate profiles, run # 2

solid lines represent molar concentration of suspended precipitate
dashed lines represent molar concentration of deposited precipitate

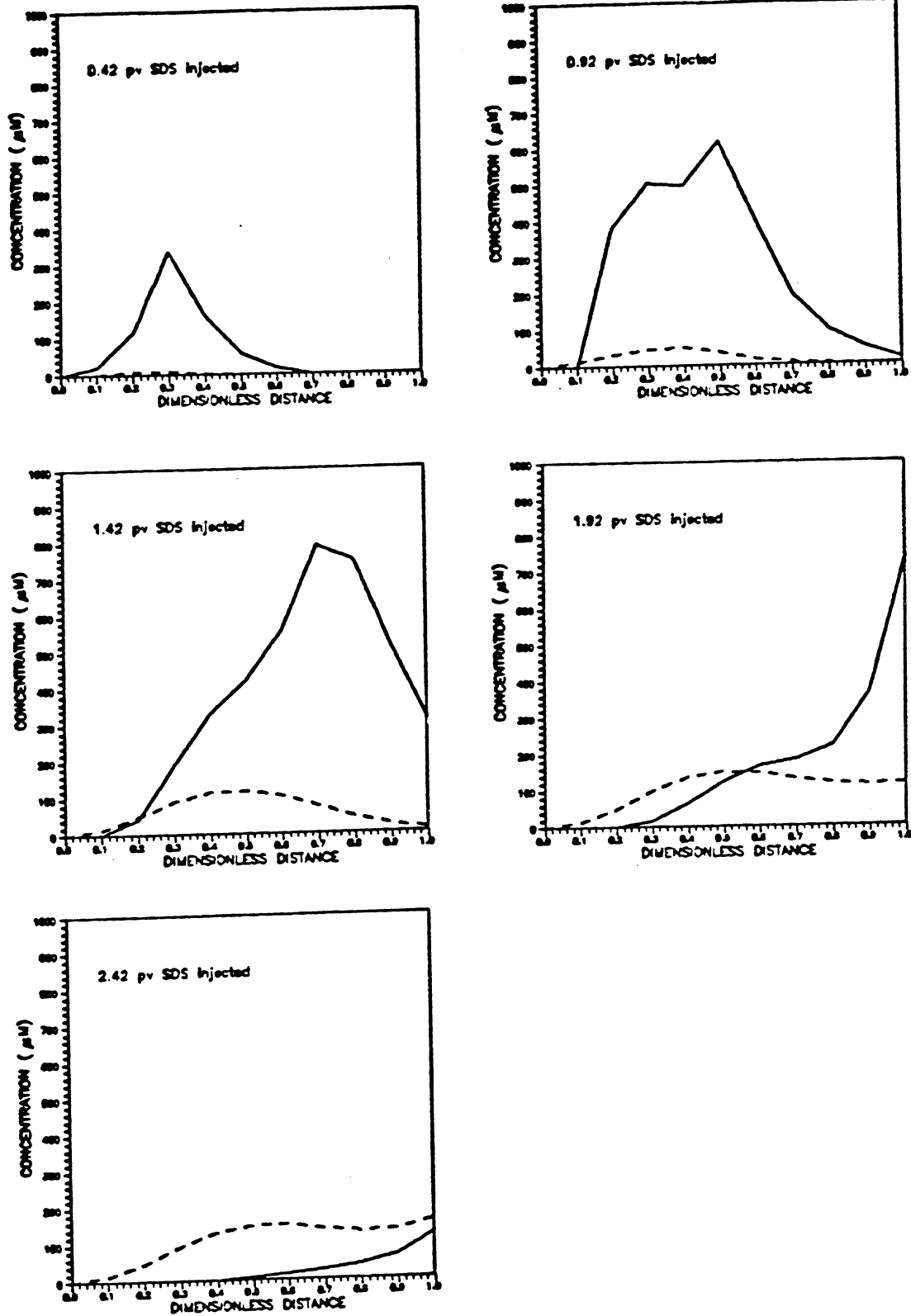


Figure 17 - Precipitate profiles, run # 3

solid lines represent molar concentration of suspended precipitate
dashed lines represent molar concentration of deposited precipitate

NOMENCLATURE

a	specific surface area, cm^2/cm^3
A	surface area, cm^2
B°	rate of nucleation, # of nuclei/ cm^3 sec
c	a pre-exponential constant, # of nuclei/ cm^3 sec
c_p	mass concentration of suspended precipitate, g/cm^3
C	concentration, $\mu\text{mole}/\text{l}$
CMC	critical micelle concentration, $\mu\text{mole}/\text{l}$
D	dispersion coefficient, cm^2/sec
d_{pin}	injected DPC concentration, $\mu\text{mole}/\text{l}$
d_{sin}	injected SDS concentration, $\mu\text{mole}/\text{l}$
eb	pore volumes of injected brine spacer
edp	pore volumes of injected DPC
eds	pore volumes of injected SDS
f	fugacity, atm
H	Henry's law constant, $\mu\text{mole}/\text{g}$
k	permeability, md
k_1	retention coefficient, cm^2/g
k_2	entrainment coefficient, $\text{g}/\text{cm}^2 \text{ g}$
$k/$	mass transfer coefficient, $\text{g}/\text{cm}^2 \text{ sec}$
K_{sp}	solubility product constant, $(\mu\text{M})^2$
L	length of the porous solid, cm
M	mass concentration of total precipitate, g/cm^3
n	number of monomers constituting a nucleus
n	empirical constant

p	pressure, atm
pe	Peclet number
q	total surfactant adsorbed, $\mu\text{mole/g}$ of solid
R	gas constant
rs	relative supersaturation
s	supersaturation, $(\mu\text{M})^2$
t	time, sec
T	absolute temperature, k
u	bulk fluid velocity, cm/sec
v	molecular volume of nucleus, cm^3
w	regular solution theory interaction parameter
x	distance, cm
X	mole fraction of surfactant in mixed micelles (surfactant only basis)

Greek letters

σ	mass concentration of deposited precipitate, g/cm^3
τ	surface tension, erg/cm^2
K	Boltzmann's constant
β	shape factor
ϕ	porosity
μ	viscosity, cp
α	inverse of compaction factor of media
ρ	density, g/cm^3
ΔG	change in free energy, ergs/mole
θ	molar affinity, ergs/molecule

Subscripts

p	precipitate
c	porous media
g	grain
a	adsorbed surfactant
m	monomer
p,b	suspended precipitate
p,d	deposited precipitate
ds	SDS
dp	DPC
M	micelle
°	initial or reference state
t	maximum capacity
s	solid media

Superscript

T	total
+	dimensionless parameter
*	critical state or nucleation state

REFERENCES

1. Tomilson, E., Davis, S.S., and Mukhayer, G.I., in "Solution Chemistry of Surfactants" (K.L. Mittal, Ed.), vol. 1, p. 3, Plenum, New York, 1979.
2. Barry, B.W., and Russel, G.F.J., J. Pharm. Sci. 61, 502 (1972).
3. Attwood, D., and Florence, A.T., "Surfactant Systems", p. 388, Chapman and Hall, New York, 1983.
4. Tomilson, E., and Davis, S.S., J. Colloid Interface Sci. 66, 335 (1978).
5. Shah, D.O., and Schechter, R.S., Improved Oil Recovery by Surfactant and Polymer Flooding, Academic press, 1977.
6. Arshad, S.A., and Harwell, J.H., SPE paper No. 14291, presented at the 60th Annual Technical Conference of the Society of Petroleum Engineers, Las Vegas (September, 1985).
7. Meehan, D.N., Menzie, D.E., J. of Pet. Tech. 30, pp.205-209, 1978.
8. Jenneman, G.E., Knapp, R.M., McInerery, M.J., Menzie, D.E., Revus, D.E., Soc. of Pet. Engr. J. 24(1), p.33, 1984.
9. Sandiford, B.B., "Selectively Controlling Fluid Flow Through the Higher Permeability Zones of Subterranean Reservoirs", U.S. pat. Appl. No. 178911.
10. Boyd, R.N., Mriganka, M.G., J. of Am. Water Works Assc. 66, No. 2, 94, 1974.
11. Arshad, S.A., Harwell, J.H., "Experimental Verification of Water-Assisted Surfactant Flooding in Berea Sand Stone Cores", in Preparation.
12. Abdollahi, A., M.S. Thesis, The University of Oklahoma, 1987.
13. Hankins, N.P., Ph.D. Dissertation, The University of Oklahoma, 1989.
14. Harwell, J.H., Helfferich, F.G., and Schechter, R.S., AICHE J. 28(3), 448, 1982.
15. Harwell, J.H., Ph.D. Dissertation, The University of Texas at Austin, 1983.

16. Trogus, F.J., Schechter, R.S., Pope, G.A., and Wade, W.H., J. Colloid Interface Sci 70(8), 293, 1979.
17. Harwell, J.H., Schechter, R.S., and Wade, W.H., AIChE J. 31 (3), 415, 1985.
18. Scamehorn, J.F., in "Phenomena in Mixed Surfactant Systems" (J.F. Scamehorn, Ed.), Vol. 311, p. 1, ACS Symp. Ser., ACS, Washington, 1986.
19. Amente, J.C., Scamehorn, J.F., Harwell, J.H., J. Colloid Interface Sci., Submitted.
20. Stellner, K.H., Ph.D. Dissertation, The University of Oklahoma, 1987.
21. Skoog, D.A., and West, D.M., "Fundamentals of Analytical Chemistry", 2nd Edition, p. 164, Holt, Rinehart, and Winston, New York, 1969.
22. Scwen, R.V., and Leja, J., Can. J. Chem. 45, 2821, 1967.
23. Reeves, R.L., and Harkaway, S.A., in "Micellization, Solubilization, and Microemulsions" (K.L. Mittal, Ed.), Vol. 2, p. 819, Plenum, New York, 1977.
24. Hoyer, H.W., and Doerr, I.L., J. Phys. Chem. 68, 3494, 1964.
25. Walton, A.G., The Formation and Properties of Precipitates, Interscience Publishers, 1967.
26. Nielsen, A.E., Kinetics of Precipitation, The McMillan Company, New York, 1964.
27. Randolph, A.D., Larson, M.A., Theory of Particulate Processes, Academic Press, Inc., 1988.
28. Zettlemoyer, A.C., Nucleation, Marcel Dekker, Inc., New York, 1969.
29. Volmer, M., and Weber, A., Z. Physik. Chem. Phys. 119, 277-301, 1926.
30. Nielsen, A.E., Acta Chem. Scand. 15, 441-442, 1961.
31. Laudise, R.A., The Growth of Single Crystals, Prentice-Hall, Inc., 1970.
32. Bradsley, W., Hurle, D.T.J., and Mullin, J.B. ed., Crystal Growth: A Tutorial Approach, North Holland Publishing Company, 1977.

33. Gruesbeck, C., Collins, R.E., Soc. of Pet. Engr. J. 847, 1982.
34. Herzig, J.P., Leclerc, D.M., Goff, P.L., Flow of Suspensions Through Porous Media- Application to Deep Filtration, ACS symp. Ser., ACS, Washington, 1969.
35. Cernansky, A., and Siroky, R., Intern. Chem. Engr 25, No.2, 364, 1985.
36. Ives, K.J., Pienvichitr, V., Chem. Eng. Sci.20, 945-973, 1965.
37. Sakthivadivel, R., Tech. Rep. HEL 15-5, Hydraulic Eng. Lab., University of California, Berkeley, 1966.
38. Civan, F., and Knapp, R.M., J. of Pet. Sci & Eng., to appear in October 1989 issue.
39. Ornatskii, N.V., Sergeev., E.M., and Shekhtman, Yu.M., Investigation of the Process of Clogging of Sands, University of Moscow, 1955.
40. Adin, A., Filtration and Separation 15, 1978.
41. Barton, J.W., Fitzgerald, T.P., Lee, C., O'Rear, E.A., and Harwell, J.H., Separation Sci. & Tech. 23(6 & 7), pp. 637-660, 1988.
42. Ruthven, D., Principals of Adsorption, 1984.
43. Arshad, S.A., Harwell, J.H., "Optimum Injection Strategies for Surfactant- Assisted Waterflooding Project", in preparation.
44. Carman, P.C., Trans. Amer. Inst. Chem. Eng. 15, 150-166, 1937.

APPENDIX A

Development of an Empirical Relation for Permeability

Permeability of a porous media can be related to pressure drop by the use of Darcy's law.

$$\frac{dp}{dx} = -u \frac{\mu}{k} \quad (A-1)$$

or

$$\frac{dp}{dp_0} = \frac{k_0}{k} \quad (A-2)$$

where the subscript \circ denotes a reference state.

The Kozeny-Carman equation is used to obtain a theoretical relation between p and σ (44).

$$\frac{dp}{dp_0} = \left[\frac{a_c}{a_{c,0}} \right]^2 \left[\frac{\phi_0}{\phi} \right]^3 \quad (A-3)$$

where a_c is the specific surface of the porous media and can be replaced by the grain specific surface (a_g),

$$\frac{a_c}{a_{c,0}} = \frac{a_g}{a_{g,0}} * \frac{1-\phi}{1-\phi_0} \quad (A-4)$$

According to the Hydraulic radius model of Skthivadivel (38), the diameter of the grain surface can be assumed to be constant and thus, a_g remains unchanged. Then,

$$\frac{a_c}{a_{c,0}} = \frac{1-\phi}{1-\phi_0} \quad (A-5)$$

We further assume that porosity, ϕ , decreases with the accumulation of the precipitate particles at the surface by the following empirical relation:

$$\phi = \phi_0 - [\alpha \sigma / \rho_p]^n \quad (A-6)$$

where α is the coefficient that accounts for the surface of the media not available to the suspended particles to be deposited. Dead end pores or regions with low potential surface sites are such regions that do not participate in the flow process. n is an empirical factor introduced to magnify the effects of deposited materials on changes in porosity, pressure drop, or permeability. This factor was also used in other studies to account for the lumped effects of mechanical and physicochemical means of plugging of a porous solid (35,39,40). When we combine equations (A-2) through (A-6) the empirical relation for the permeability is obtained as follows:

$$\frac{k}{k_0} = \frac{[1 - (\sigma/\sigma_t)^n]^3}{[1 + (\phi_0/1-\phi_0) (\sigma/\sigma_t)^n]^2} \quad (\text{A-7})$$

where σ_t is the maximum capacity of the media and is found by taking a zero porosity.

$$\sigma_t = \frac{(\phi_0)^{1/n} \rho_p}{\alpha} \quad (\text{A-8})$$

